Graduate School Form 30
Updated 1/15/2015

PURDUE UNIVERSITY
GRADUATE SCHOOL
Thesis/Dissertation Acceptance

This is to certify that the thesis/dissertation prepared

By Zhibin Song

Entitled

Modeling and Simulation of Heat of Mixing in Li Ion Batteries

For the degree of Master of Science in Mechanical Engineering

Is approved by the final examining committee:

Likun Zhu
Chair

Jian Xie

Hazim EI-Mounayri

To the best of my knowledge and as understood by the student in the Thesis/Dissertation Agreement, Publication Delay, and Certification Disclaimer (Graduate School Form 32), this thesis/dissertation adheres to the provisions of Purdue University's "Policy of Integrity in Research" and the use of copyright material.

Approved by Major Professor(s): Likun Zhu

Approved by: Jie Chen 7/27/2015

Head of the Departmental Graduate Program Date

MODELING AND SIMULATION OF HEAT OF MIXING IN LI ION BATTERIES

A Thesis

Submitted to the Faculty

of

Purdue University

by

Zhibin Song

In Partial Fulfillment of the

Requirements for the Degree

of

Master of Science in Mechanical Engineering

August 2015

Purdue University

Indianapolis, Indiana

ACKNOWLEDGMENTS

I would like to gratefully acknowledge my advisor, Dr. Likun Zhu, for his supervision, guidance, and scientific support during the entire course of this research and thesis work. Dr. Zhu generously shared with me his research experience and academic approaches.

I would also like to appreciate my advisory committee members, Dr. Jian Xie and Dr. EI-Mounayri for their time and insight during the completion of my thesis.

I would like to expand my special thanks to my collaborators Dr. Yan Bo, Cheolwoong Lim, Yuanzhi Cao for their fruitful discussions and valuable contributions that led to successful completion of the research.

Finally, I would like to dedicate this manuscript to my family. Without their love and support I would not have made this far.

This research is supported by the donors of the American Chemical Society Petroleum Research Fund.

TABLE OF CONTENTS

Page

LIST OF TABLES

LIST OF FIGURES

ABSTRACT

Song, Zhibin. M.S.M.E., Purdue University, August 2015. Modeling and Simulation of Heat of Mixing in Li Ion Batteries. Major Professor: Likun Zhu.

Heat generation is a major safety concern in the design and development of Li ion batteries (LIBs) for large scale applications, such as electric vehicles [1]. The total heat generation in LIBs includes entropic heat, enthalpy, reaction heat, and heat of mixing [2]. The main objective of this study is to investigate the influence of heat of mixing on the LIBs and to understand whether it is necessary to consider the heat of mixing during the design and development of LIBs [3]. In the previous research, Thomas and Newman derived methods to compute heat of mixing in LIB cells. Their results show that the heat of mixing cannot be neglected in comparison with the other heat sources at 2 C rate [4].

In this study, the heat of mixing in different materials, porosity, particle sizes, and charging/discharging rate was investigated. A COMSOL mathematical model was built to simulate the heat generation of LIBs. The LIB model was based on Newmans model. $LiMn_2O_4$ and $LiCoO_2$ were applied as the cathode materials, and LiC_6 was applied as the anode material [5]. The results of heat of mixing were compared with the other heat sources to investigate the weight of heat of mixing in the total heat generation. The heat of mixing in cathode is smaller than the heat of mixing in anode, because of the diffusivity of $LiCoO_2$ is $1 \times 10^{-13}\ m^2/s$, which is larger than LiC_6's diffusivity $2.52 \times 10^{-14}\ m^2/s$. In the comparison, the heat of mixing is not as much as the irreversible heat and reversible heat, but it still cannot be neglected.

Finally, a special situation will be discussed, which is the heat of mixing under the relaxation status. For instance, after the drivers turn off their vehicles, the entropy,

enthalpy and reaction heat in LIBs will stop generating, but the heat will still be generated due to the release of heat of mixing. Therefore, it is meaningful to investigate to see if this process has significant influence on the safety and cycle life of LIBs.

1. INTRODUCTION

1.1 Overview of Li Ion Batteries

The Li ion battery is a kind of secondary battery (rechargeable battery), which mainly depends on the work of moving of the Li ions between the positive electrode and the negative electrode. In the charge process, the Li ions deintercalate from the positive electrode and move to the negative electrode through the electrolyte. In the discharge process, the Li ions deintercalate from negative electrode and move to the positive electrode through the electrolyte [6]. Materials containing Li ions are commonly used as the electrode element. The LIB is representative of modern high-performance batteries. The positive electrode half-reaction is:

$$\mathrm{LiCoO_2} \leftrightarrows \mathrm{Li_{1-x}CoO_2} + x\mathrm{Li^+} + x\mathrm{e^-}$$

The negative electrode half reaction is:

$$x\mathrm{Li^+} + x\mathrm{e^-} + x\mathrm{C_6} \leftrightarrows \ x\mathrm{LiC_6}$$

Li ion batteries have been industrialized since 1992. The market increased rapidly. Its growth rate is ten times that of the lead-acid battery. The rapid development of the Li ion batteries attracted great interest in the electric vehicle industry. With Li ion batteries applied in electric vehicles, the safety issues in the vehicles with a large capacity, high power LIB and battery pack got more and more attention. Although the Li ion batteries safety has been greatly improved compared to the lithium batterys safety, as a vehicle power source, lithium ion batteries still have many safety risks, especially to the battery under abusive conditions (overcharge, pinning, extrusion voltage, short circuit, etc.) [7, 8] The safety issue has become the bottleneck of the wide use of Li ion batteries in electric vehicle.

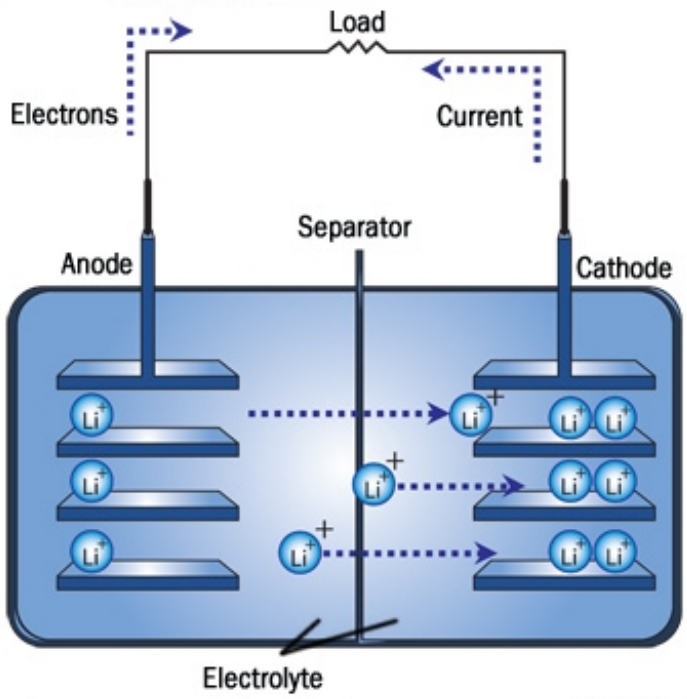

Figure 1.1. Li ion battery discharge mechanism

Li ion battery safety is highly concerned, and it's closely related to the desired application. The application of Li ion batteries in electric vehicle, regardless of the level of single capacity, must use a combination of the batteries. In any use of the process of a single battery over charge or over discharge, particularly for a high - capacity battery, no thermal disturbance are likely to exceed the battery limitation of the material thermally stable state and ultimately lead to thermal runaway and cause safety problems. Due to urgent need of low - carbon economy and green energy development, countries have been using the Li ion batteries for electric energy. Thus, in order to promote the rapid and healthy development, to carry out the Li ion battery safety, as well as analyze the thermal properties for realistic using, Li ion battery

thermal characteristics and extended methodology is undoubtedly very important and urgent.

Thermal behavior of Li ion batteries has been studied for a long time due to their risks of explosion under high temperature and problems for thermal runaway. The thermal sources in Li ion batteries include resistive heat, reaction heat, entropic heat, and heat of mixing. In this research, the heat of mixing was mainly discussed. Heat of mixing is also called enthalpy of mixing [4]. It is a small heat source, but can exist although the charge and discharge process have been stopped.

Heat of mixing is the heat that is taken up or released upon mixing of two (non-reacting) chemical substances. When the enthalpy of mixing is positive, mixing is endothermic while negative enthalpy of mixing signifies exothermic mixing [9,10]. In ideal mixtures the enthalpy of mixing is null. In non-ideal mixtures the thermodynamic activity of each component is different from its concentration by multiplying with the activity coefficient.

In other words, heat of mixing is the difference between the enthalpy of a mixture and the sum of the enthalpies of its components at the same pressure and temperature. When two liquids are mixed, the final enthalpy is not necessarily the sum of the pure component enthalpies. This is because the unlike interactions between molecules is most likely different than the like interactions. Thus, if the A - B interactions are stronger than the A - A and B - B interactions, then the mixing process will be exothermic (heat will be released because the more tightly bound A - B interactions are at a lower energy).

In the previous researches, heat of mixing is a small source to compare with the total heat generation, so that it might be ignored at some time. However, the heat of mixing does not only exist during the charging and discharging process, but also exists after the charging and discharging process have been finished. Thats the most significant reason to investigate it. The objective of this research is to find the important factors of heat of mixing, and find out the rules that how do they influence the heat of mixing.

The calculation of heat of mixing had been done by previous literatures. Newman and Thomas did recognized work with this topic. In this research, we are trying to do several things:

- Making clear how the parameters will influence the heat of mixing specifically.
- Doing integration for the current, but not assume it as a constant in the pseudo 2D model simulation.
- Calculating heat of mixing using the new result of the current density.
- Trying to make a 3D structure model and investigate the thermal behavior.

Therefore, this is a work about the investigation of the property of heat of mixing and simulation in an advanced method.

1.2 Literature Review

The heat generation problem has been studied for a long period due to it is being a significant factor to the cycle life and security of the Li ion batteries. In a paper from Newman and Thomas, they also tried to simulate the heat of mixing of cathode in Li ion batteries. Newman's model was applied in that research, and the model was built for a half cell [2]. Through the simulation, they got the results of heat of mixing in 1/3 C, 1 C, and 2 C rate, and compared them to the other heat sources.

In the results from Thomas's paper, heat of mixing has the same magnitude as the irreversible and reversible heat. At that time, people cannot know the concentration change within the particles clearly, so they assumed the concentration change within particles is linear. The same assumption was also made for the concentration across the electrode [2]. Nowadays, we have many ways to monitor the concentration change in cathode, even in micro scale, and have advanced simulation software, so a more detailed and advanced simulation should be done. Kumaresan and R.E White obtained the open-circuit potential vs state-of-charge profiles of $LiCoO_2$ and MCMB by

conducting half cell tests. They got entropy of $LiCoO_2$ and MCMB as a function of state of charge [5]. The detailed mathematical measurement was discussed in another paper from Thomas and Newman. The experimental results also used in this research. Based on the experimental results, Kumaresan built a thermal model to simulate the discharge performance of the Lithium ion batteries at different temperatures and C rates.

After that, Cai and White built a mathematical model of Li ion batteries with thermal effect in COMSOL. In the simulation, the cell voltage, concentration of electrolyte, and the temperature on the cell surface were investigated. They proved that the thermal behavior of a lithium ion battery during discharge can be predicted by using COMSOL [11]. The success of their research made us mind to use COMSOL to do the thermal simulation of heat of mixing in Lithium ion batteries.

Heat of mixing also mentioned in Zhang's doctoral thesis [12]. A clear process of how to calculate dH/dC was conducted in the thesis. He also used the Newman's model and assumed the spherical particles are uniform in the electrodes. Averaged heat generation rates were obtained by simulation in two cases. The averaged generation rate of heat of mixing was -7.55×10^{-14} W and -2.31×10^{-13} W when the potential sweep rate was 0.4 mV/s and 1 mV/s [12].

Kim and Park modeled for the thermal behavior of a Li ion battery during charge process. They built the whole electrodes, and connected positive electrode and negative electrode node by node. In this way, they can investigate the heat transfer between electrodes [13]. The simulation results showed temperature distributions based on experimental image and modeling. It is meaningful if we continue to investigate heat of mixing transfer and compare to their results.

Baba and Kawauchi also built a model to do numerical simulation of thermal behavior of Li batteries by using single particle model. In their model, each of negative and positive electrodes is represented by a single spherical particle in the electrolyte phase. The physical quantities are approximated by parabolic profiles within each

electrode [14]. Therefore, it limited to show the heat of mixing across electrolyte and electrode. Thats a reason we choose the Newmans model.

To know more about the heat generation in Li ion batteries, we checked Jiang and Sun's paper. They did thermal analyses of $LiFePO_4$/graphite battery for discharge process. Joule Heat, reversible entropy heat and ionic migration heat were shown as results in the paper [15]. We didn't apply $LiFePO_4$ in this research, but it is meaningful to compare the results with them to know the differences between materials.

To show the properties of heat of mixing, $LiCoO_2$ and $LiMn_2O_4$ were taken as the cathode materials, and LiC_6 was taken as anode material.

Lithium cobalt oxide was first proposed by Mizushima as a Li ion battery cathode material. The theoretical specific capacity is 274 mAh/g, but currently its actual specific capacity is about 140 mAh/g [5]. Because its production process is simple and electrochemical properties are stable, it captured market quickly. The Lithium cobalt oxide material has a high voltage, steady discharge curve for large current, high specific energy, and its structure is good for lithium ions transfer.

Lithium manganese oxides theoretical specific capacity is 283 mAh/g, but the actual specific capacity is between 110 to 120 mAh/g. Its advantage are good stability, non-polluting, high voltage, and low cost. Currently the applications are mostly $LiMn_2O_4$ in Spinel type, having a three-dimensional tunnel structure. The average operating voltage of $LiMn_2O_4$ is about 3.8 V [12].

1.3 Mathematical Model

The pseudo 2D Li-ion cell model consists of three regions - the negative composite electrode (with LiC_6 active material), an electron-blocking separator, and positive composite electrode (with $LiCoO_2$ active material). During discharge, lithium ions inside of solid LiC_6 particles diffuse to the surface where they react and transfer from the solid phase into the electrolyte phase. The positively charged ions travel

via diffusion and migration through the electrolyte solution to the positive electrode where they react and insert into solid metal oxide particles [16]. Electrons follow an opposite path through an external circuit or load. Here, we briefly summarize that pseudo 2D electrochemical model and introduce the coupled lumped thermal model.

Figure 1.2. Geometry of Li ion battery pseudo 2D model

As we can see in Figure 2, the software separates the model into three regions. The left part is the anode, the middle part is the separator, and the right part is the cathode. The length of the each part represents the thickness for them. Different from the 1D model, the pseudo 2D model assumes that each region was constructed by particles. The black points we can see in the anode and cathode region are the particles selected in this model.

For easy calculation, we assume the particles in the model are uniformly spherical. The spherical particle was constructed by 20 spherical layers. In COMSOL software, the concentration for each layer within the particles can be known. The concentration difference from the surface to center of a particle will lead to enthalpy change, which is the heat of mixing within the particles.

Moreover, because the current density is not a constant across the electrode thickness, the integration for the current density needs to be done before the heat of mixing across electrode and electrolyte calculation.

1.3.1 Governing Equations

Based on the Newman's model, the final form of the heat generation is:

$$Q = I\left(V - U^{avg}\right) + IT\frac{\partial U^{avg}}{\partial T} + \sum_{k} H_k^{avg} r_k + \int \sum_{j}\sum_{i}\left(H_{ij} - H_{ij}^{avg}\right)\frac{\partial c_{ij}}{\partial t}dv \quad (1.1)$$

where Q is the heat transferred from the surroundings to the battery system, V is the cell potential, U is the thermodynamic (open-circuit) potential and evaluated at the average state of charge in the electrodes, T is the temperature, I is the current (positive on discharge), which is obtained by the integration of current density i_n, c_{ij} is the concentration of species i and is a function of position and time; H_{ij} is the partial molar enthalpy, which is a function of composition, pressure, and temperature; and the integral is over the entire volume of the system [2].

In the Equation (1.1), the first term on the right side is the irreversible resistive heating, which is caused by the deviation of the cell potential from its equilibrium potential by the resistance of the cell to passage of current. The second term is the reversible entropic heat, the third term is heat change by any chemical reactions that may be present in the cell, and the last term is the heat of mixing.

The goal of this research is to investigate the last term in the above equation. Through the deviation in the Thomass paper, the part of heat of mixing could be written as below:

Heat of mixing within particles:

$$Q_{mixing} = \frac{\partial}{\partial t}\left[\frac{1}{2}\frac{\partial H_s}{\partial C_s}\int (C_s - C_{s,\infty})^2 dv\right] \tag{1.2}$$

$$\frac{\partial H_s}{\partial C_s} = -F\frac{\partial U_H}{\partial C_s} \tag{1.3}$$

$$\mathrm{U_H = U - TdU/dT} \tag{1.4}$$

The dH/dC is obtained by numerical differentiation of U_H over concentration, where U_H is the enthalpy potential, C_s is the local concentration, F is Faraday constant, dU/dT is measured concentration, and is thus dependent upon state of charge [12]. The experimental results of U and dU/dT from the Reference are used at here [5].

Figure 1.3 and Figure 1.4 show the open circuit potential of $LiCoO_2$ and LiC_6. Because the cell voltage cannot reach a very low point, 3.6 V was selected to be the

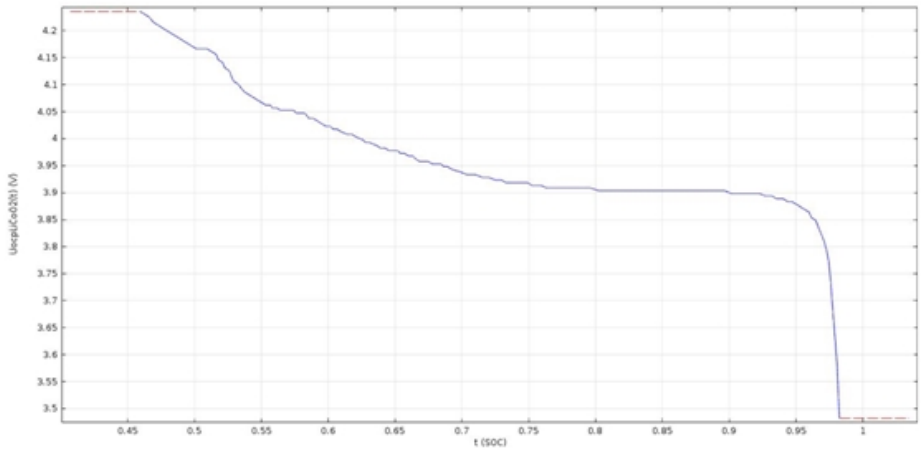

Figure 1.3. Open circuit potential of Li_xCoO_2 vs state of charge [5]

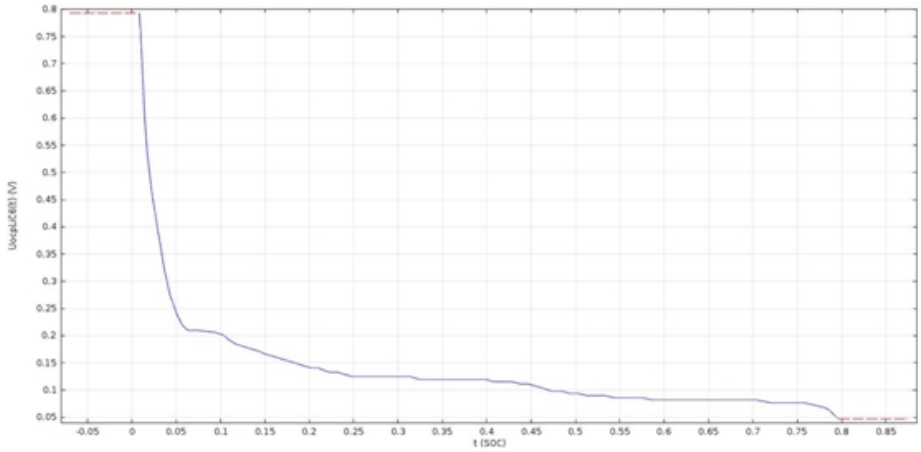

Figure 1.4. Open circuit potential of Li_xC_6 vs state of charge [5]

stop condition for the discharging process. Based on this condition, 0.5 - 0.95 SOC period of the $LiCoO_2$ and 0.28 - 0.78 SOC of the LiC_6 were selected to use.

Figure 1.5 and Figure 1.6 are the derivative of OCP over temperature. Then, based on the curve fit on Figure 1.3 to Figure 1.6, the derivative of partial molar enthalpy over concentration can be obtained by Equation (1.2-1.4), so that the important data dH/dC can be derived by integration.

Based on the results of the simulation, the concentration at each layer can be known. Then, we can do integral for the direction from center to surface of a particle.

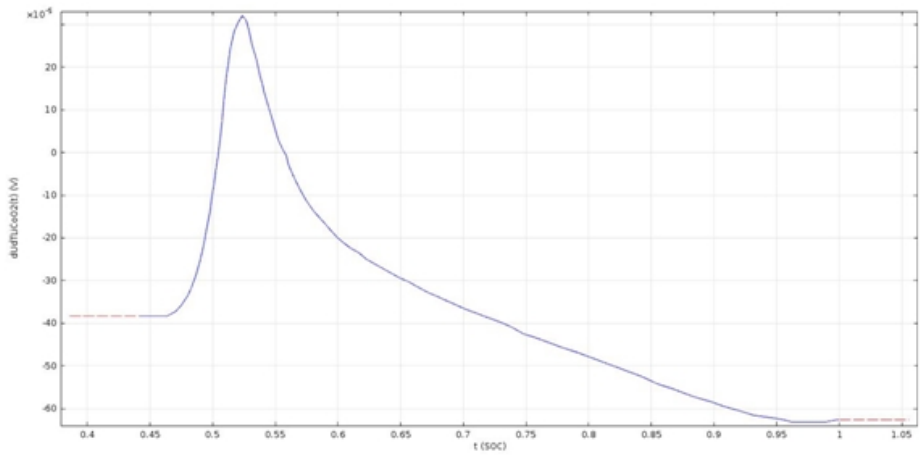

Figure 1.5. dU/dT of Li_xCoO_2 [5]

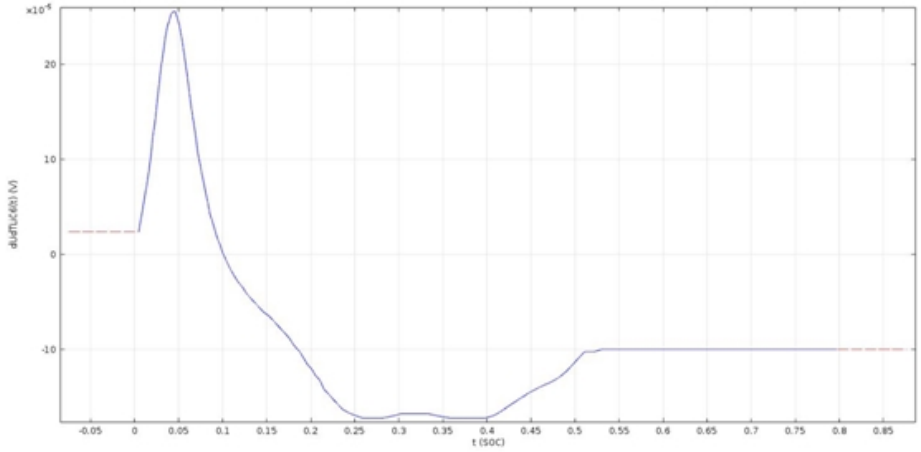

Figure 1.6. dU/dT of Li_xC_6 [5]

Heat of mixing within particles:

$$C = \frac{l-x}{l}C_1 + \frac{x}{l}C_2; l = r_2 - r_1 = \frac{R}{n} \tag{1.5}$$

where C is local concentration, C_1 is the first layer concentration next to the particle center, C_2 is the concentration at next layer, l is the length between each layer, r_2 and r_2 is the radius at different layers. The assumption is the concentration is linear increasing or decreasing between each connected layer. Because there are 20

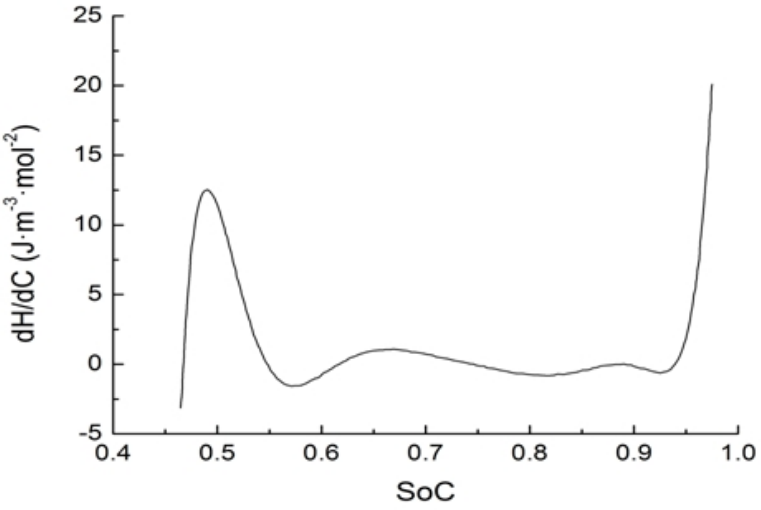

Figure 1.7. The derivative of partial molar enthalpy over concentration of $LiCoO_2$

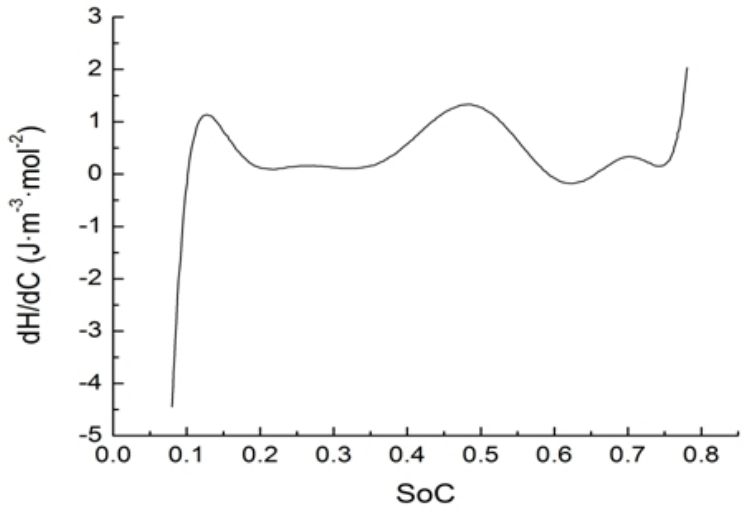

Figure 1.8. The derivative of partial molar enthalpy over concentration of LiC_6

layers for a particle, the elemental length is only 0.1 μm for the $LiCoO_2$ particles, so that the error caused by the linear assumption is neglected.

Then, we can go ahead to do the integral part in the equation (1.2)

$$\int_{r_1}^{r_2} (C - C_\infty)^2 4\pi r^2 dr \tag{1.6}$$

$$= \frac{1}{l^2} \int_{r_1}^{r_2} \left[(C_1 - C_\infty)\, l + x\,(C_2 - C_1) \right]^2 4\pi r^2 dr \tag{1.7}$$

$$= \frac{1}{l^2} \int_{r_1}^{r_2} \left[l^2 (C_1 - C_\infty)^2 + 2l\,(C_1 - C_\infty)\, x\,(C_2 - C_1) + r^2 \left(C_2 - C_1\right)^2 \right] 4\pi r^2 dr \tag{1.8}$$

$$= (C_1 - C_\infty)^2 \frac{4\pi r^3}{3} \Big|_{r_1}^{r_2} + \frac{2}{l}\,(C_1 - C_\infty)\,(C_2 - C_1)\, 4\pi \frac{r^4}{4} \Big|_{r_1}^{r_2} + \frac{r^5}{5l} 4\pi (C_2 - C_1)^2 \Big|_{r_1}^{r_2} \tag{1.9}$$

The Equation (1.9) is the final form we get for the heat of mixing within particles.

For the heat of mixing across the electrolyte and electrode, the integral is different from the previous one.

Heat of mixing across electrode or electrolyte:

$$\int_{-d/2}^{d/2} (C - C_\infty)^2 dv = \int_{-d/2}^{d/2} (C - C_\infty)^2 dx \tag{1.10}$$

$$C = C_1 + \frac{x}{d}\,(C_2 - C_1) = \frac{(d - x)}{d} C_1 + \frac{x}{d} C_2 \tag{1.11}$$

$$= \int_{-d/2}^{d/2} \left(\frac{d - x}{d} C_1 + \frac{x}{d} C_2 - C_\infty \right)^2 dx \tag{1.12}$$

$$= \frac{1}{d^2} \int_{-d/2}^{d/2} \left[d\,(C_1 - C_\infty) + x\,(C_2 - C_1) \right]^2 dx \tag{1.13}$$

$$= \frac{1}{d^2} \int_{-d/2}^{d/2} \left[d^2 (C_1 - C_\infty)^2 + 2d\,(C_1 - C_\infty)\, x\,(C_2 - C_1) + x^2 (C_2 - C_1)^2 \right] dx \tag{1.14}$$

$$= d(C_1 - C_\infty)^2 + \frac{x^3}{3} (C_2 - C_1)^2 \frac{1}{d^2} \Big|_{-d/2}^{d/2} \tag{1.15}$$

$$= d(C_1 - C_\infty)^2 + \frac{d}{12}(C_2 - C_1)^2 \tag{1.16}$$

Where d is the element length of electrode, the electrode was separated by 40 elements. The element length depends on the electrode thickness.

There is also heat of mixing within pores, but we can know it is quite small from the Thomass paper, not even in the same magnitude with other heat of mixing source. Therefore, it was not considered at here, but the equations are shown below:

Heat of mixing within pores:

$$\mathrm{H} = \frac{1}{\mathrm{C}_{0,\infty}\mathrm{V}_{0,\infty}}\frac{\partial \mathrm{H}}{\partial \mathrm{C}}|_\infty \left(\frac{\mathrm{I}}{\mathrm{FD}}\right)^2 \frac{\varepsilon^3}{\mathrm{L}} \left(\frac{\mathrm{R}}{\varepsilon_{\mathrm{insertion}}}\right)^4 \frac{1}{1944} \tag{1.17}$$

$$\mathrm{H} = \frac{1}{\mathrm{C}_{0,\infty}\mathrm{V}_{0,\infty}}\frac{\partial \mathrm{H}}{\partial \mathrm{C}}|_\infty \left(\frac{\mathrm{I}}{\mathrm{FD}}\right)^2 \frac{\pi}{96}\mathrm{R}^4\mathrm{L} \tag{1.18}$$

To investigate the heat of mixing, we need to know how it is compared to the other heat sources, especially to the total heat generation. Therefore, the mathematical model of irreversible heat and reversible heat were also built for the research.

Irreversible heat:

$$\mathrm{H}_{\mathrm{irreversible}} = \mathrm{i}_\mathrm{n} \cdot \mathrm{s} \cdot \mathrm{n} \cdot \eta \tag{1.19}$$

Reversible heat:

$$\mathrm{H}_{\mathrm{reversible}} = \mathrm{i}_\mathrm{n} \cdot \mathrm{T} \cdot \frac{\mathrm{dU}}{\mathrm{dT}} \cdot \mathrm{n} \cdot \mathrm{s} \tag{1.20}$$

Where i_n is current density, is over potential, L is length of electrode, R is the radius of the particle.

1.3.2 Parameters, Initial Values and Stop Conditions

Table 1.1. Parameter of the $LiCoO_2$ standard discharge model

Name	Value	Description
i_1C	21[A/m^2]	1C discharge current
Ds_neg	2.52e-14[m^2/s]	Solid phase Li-diffusivity Negative
Ds_pos	1e-13[m^2/s]	Solid phase Li-diffusivity Positive
rp_neg	6e-6[m]	Particle radius Negative
rp_pos	2e-6[m]	Particle radius Positive
T	298 K	Temperature
Dl	7.5e-11[m^2/s]	Salt diffusivity in Electrolyte
epsl_pos	0.3	Electrolyte phase vol-fraction Positive
epss_pos	0.7	Solid phase vol-fraction Positive
cl_0	1000[mol/m^3]	Initial electrolyte salt concentration
epsl_neg	0.3	Electrolyte phase vol-fraction Negative
epss_neg	0.7	Solid phase vol-fraction Negative
csmax_neg	31858[mol/ m^3]	Max solid phase concentration Negative
csmax_pos	49943[mol/ m^3]	Max solid phase concentration Positive
cs0_neg	csmax_neg*0.78	Initial Negative State of Charge
cs0_pos	csmax_pos*0.5	Initial Positive State of Charge
L_neg	55e-6[m]	Length of negative electrode
L_sep	15e-6[m]	Length of separator
L_pos	50e-6[m]	Length of positive electrode

Table 1.1 included parameters and initial values for the standard pseudo 2D model. The C rate, particle radius, porosity, and thickness will change in the follow research to compare the results to this. Stop condition is decided by the cell voltage. As we can see from the Figure 1.3 and Figurer 1.4, to have stable cell voltage, the stop condition for the discharging process is lower than 3.6 V, and the stop condition for the charging process is higher than 4.2 V [17].

1.4 Validation

Because there is not experimental result to compare, to make sure the simulation results are correct, a validation is necessary.

The parameters in this validation are the same as the parameters in Thomas's paper. The only difference is the concentration distribution. In Thomas's paper, they assumed the change in enthalpy upon relaxation of pseudo-steady-state concentration gradients that were formed within spherical particles in an electrode with a uniform current distribution. However, in the real situation, the current distribution is not uniform, so in our model, the concentration gradients within spherical particles in the electrode were formed with an integral current distribution. Because of that, the results of heat of mixing in validation model might be larger than the results in Thomas's paper, but they should still have the same magnitude [2].

The basic parameters are shown below:

Negative Electrode	
Li foil thickness (μm)	750
Separator	
Area (cm^2)	1.0
Thickness (μm)	25.4
Porosity	0.47
Positive Electrode	
Thickness (μm) cell 073	181
cell 076	174
Average particle radius (μm)	20
Active material volume fraction	0.4188
Porosity	0.368
Binder plus conductive filler volume fraction	0.2132

Figure 1.9. The model parameters from Thomas's model

The results in Thomas's paper are shown below:

Table 1.2. Simulation results of Thomas's model

	C/3 for 3 h (J/m^2)
Within particles	22-110
Across electrode	0.1-19
Across electrolyte	2.0
Irreversible + entropic	7520

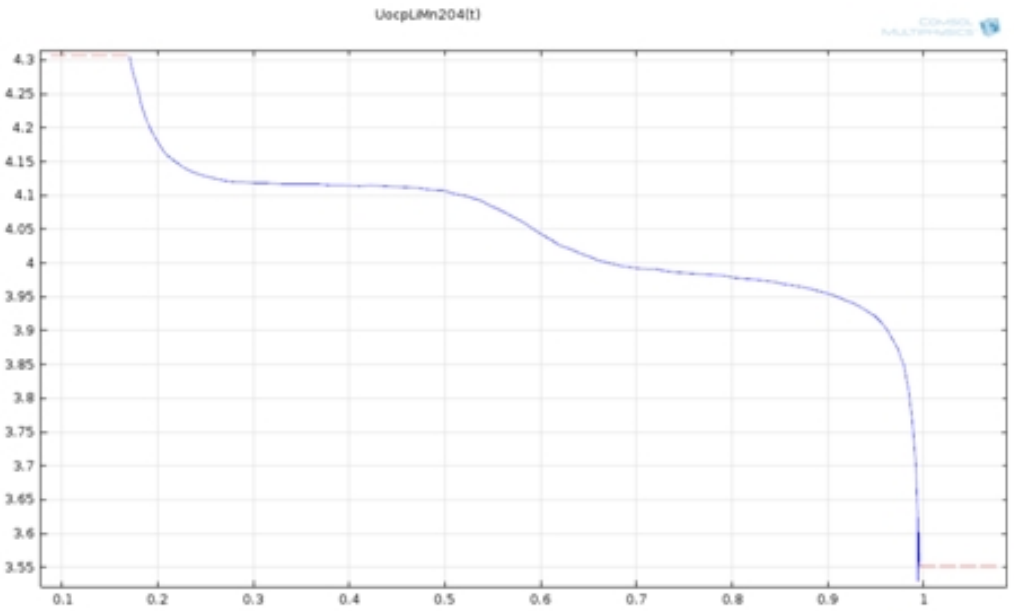

Figure 1.10. Open circuit potential of $Li_xMn_2O_4$

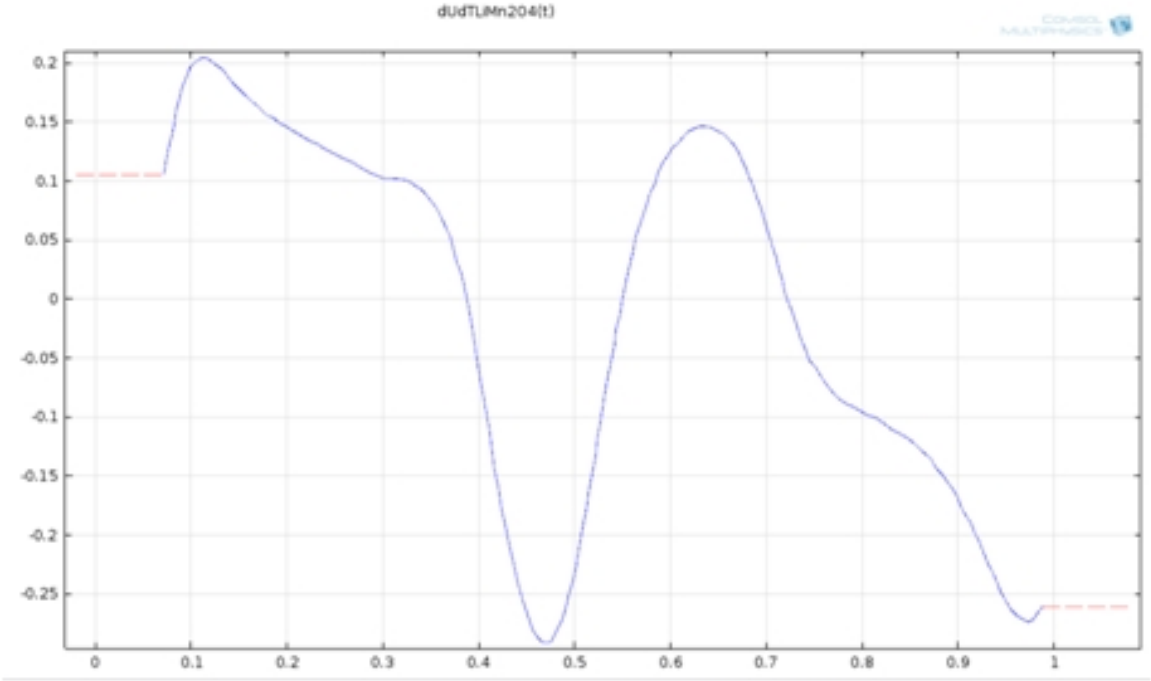

Figure 1.11. dU/dT of $Li_xMn_2O_4$

From the above figures, it is easy to find the final value of the heat of mixing, irreversible heat and entropic heat. The results are shown below:

Table 1.3. Simulation results of validation model

	C/3 for 3 h (J/m^2)
Within particles	22.8
Across electrode	0.247
Across electrolyte	9.69
Irreversible + entropic	3702

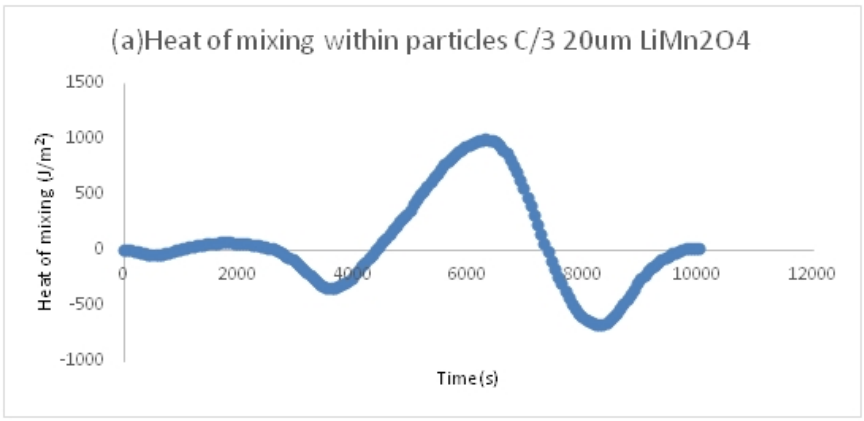

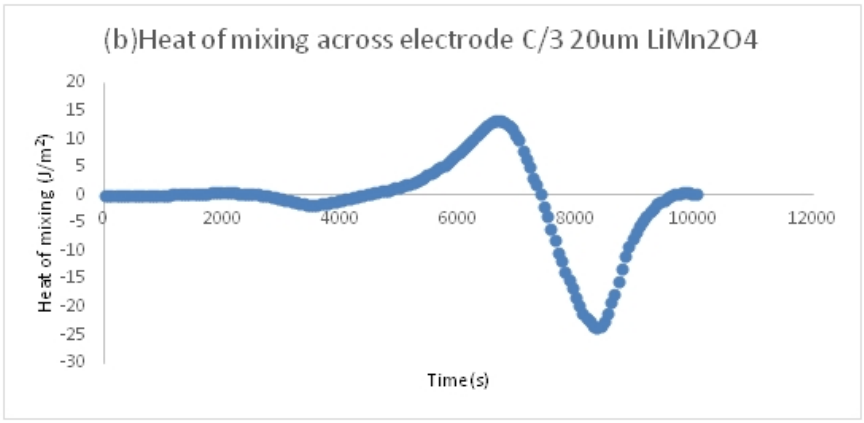

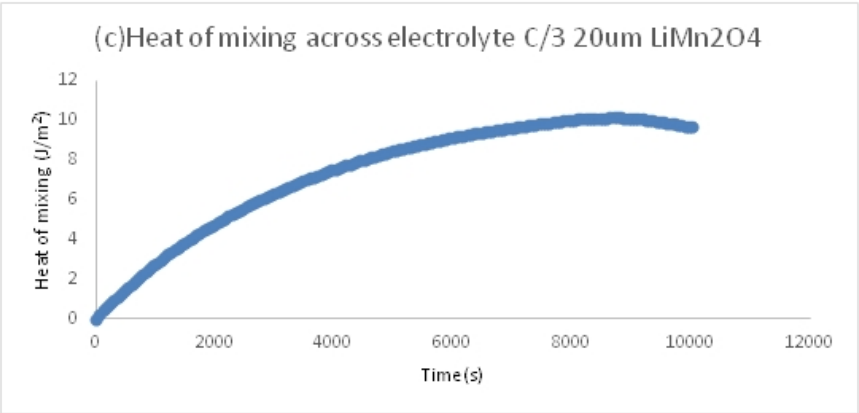

Figure 1.12. Heat of mixing results of the validation model

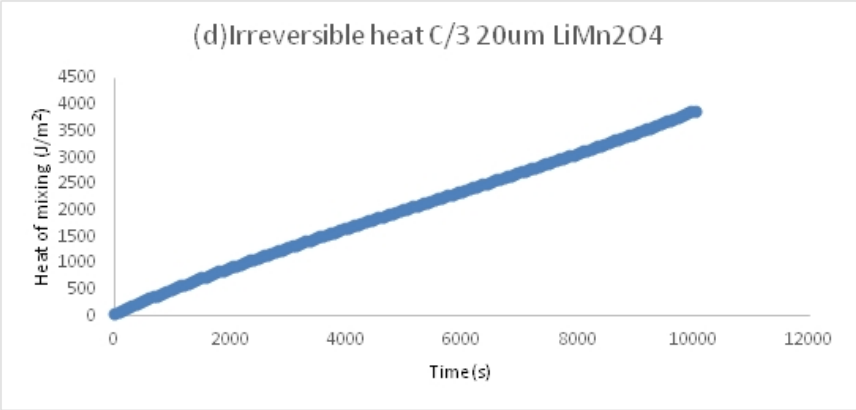

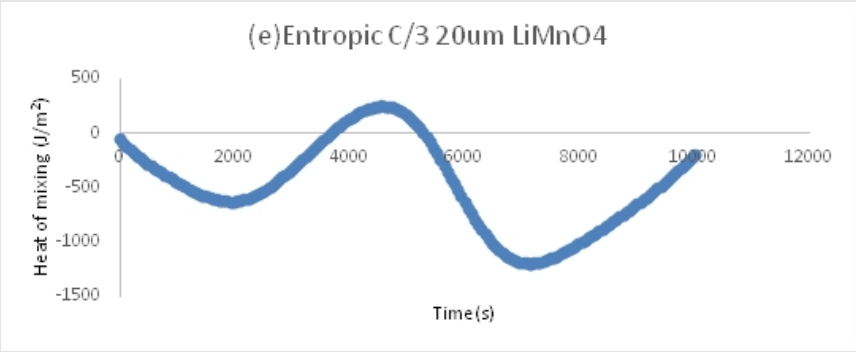

Figure 1.13. Irreversible heat and entropic results of the validation model

Compared validation results to Thomas's results in Table 1.2, the heat of mixing within particles and the heat of mixing across electrode are in the estimated range of Thomas's results. The heat of mixing across electrolyte is larger than it is in Thomass model is because the electrolyte salt concentration change is not uniform.

The electrolyte salt concentration change in validation model is shown below:

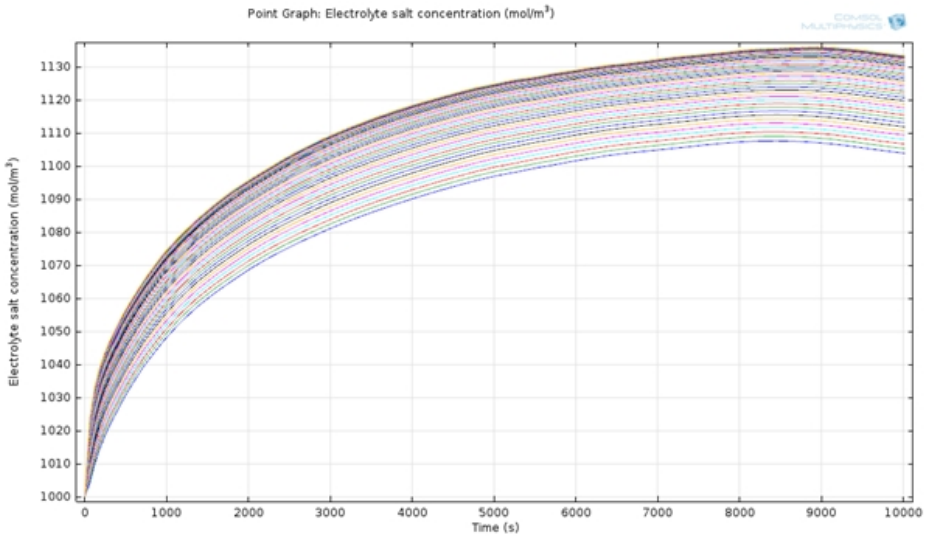

Figure 1.14. Electrolyte salt concentration change in validation model

2. RESULTS AND DISCUSSION

2.1 Investigation on Lithium Cobalt Oxide

$LiCoO_2$ is what we were mainly focused on in this research. It is widely used in various areas, which include electric vehicles, cell phones, laptops, etc. Tesla Motor Model S used the $LiCoO_2$ batteries as its power source instead of the traditional petroleum.

To investigate the heat of mixing generation, a standard model should be used to compare with the heat generation under different parameter conditions.

Table 2.1. Main parameters for the standard model of Li ion battery

	Cathode ($LiCoO_2$)	Anode (LiC_6)
Diffusion coefficient	1×10^{-13}	2.52×10^{-14}
Particle radius	2 μm	6 μm
Porosity	0.3	0.3
Maximum concentration	49943 mol/m^3	31858 mol/m^3
Temperature	298K	
Thickness	50 μm	55 μm

Figure 2.1 shows the primary results that we get from the model using standard parameters. The magnitude of heat of mixing within particles is almost ten times smaller than the heat of mixing across electrode and electrolyte. It is because the concentration gradient from particle surface to the center is much smaller than the concentration gradient across the electrode.

2.1.1 Result for The Standard Model

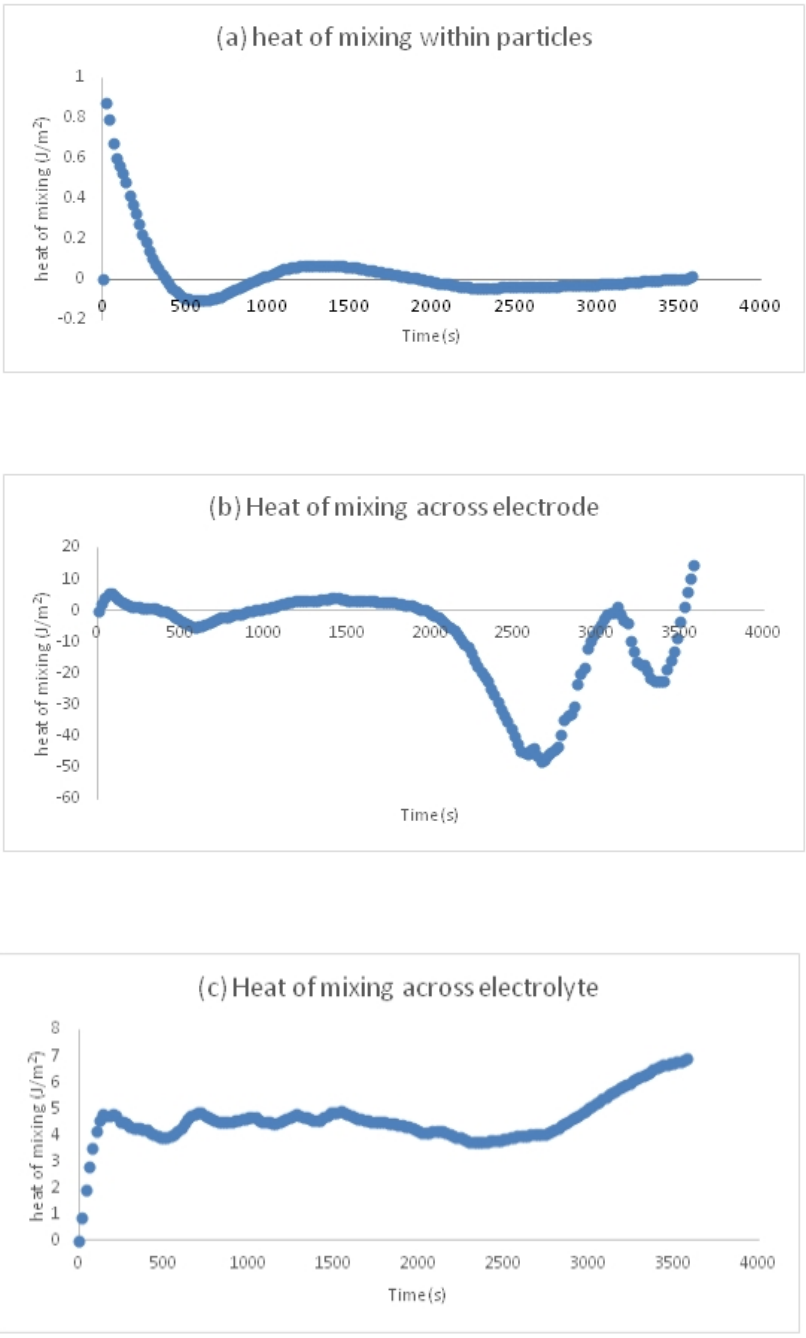

Figure 2.1. Heat of mixing within particles, heat of mixing across electrode and heat of mixing across electrolyte from the standard model

To analyze the results, the Figure 2.1(a) shows a high value at the beginning of the curve. It is due to the high value at the beginning of the dH/dC of $LiCoO_2$ which we can check in Figure 1.7. The concentration difference between two layers within the particle is only 8-10 mol/m_3. Because the concentration difference within the particles between each two adjacent layers is small, the curve trend of the heat of mixing within particles is highly similar to the curve of dH/dC of $LiCoO_2$. The small concentration gradients also lead to the small magnitude of the heat of mixing values.

Figure 2.1(b) shows the heat of mixing across the electrode. There are two valleys at the second half of the discharge process. They come from the concentration change during the discharge. Figure 2.2 shows the concentration change within the particle by time.

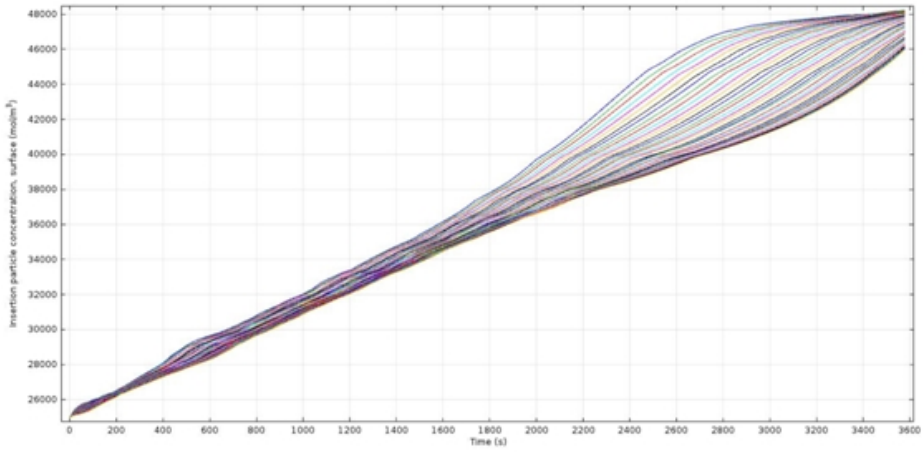

Figure 2.2. Li ion concentration change along the electrode

The curves represent different position points that are selected along the electrode from separator to current collector. It is easy to see that the concentration difference become larger in the second half of the discharging process. Based on this and the equation (2) we can explain the jump in the second half of the heat of mixing across electrode.

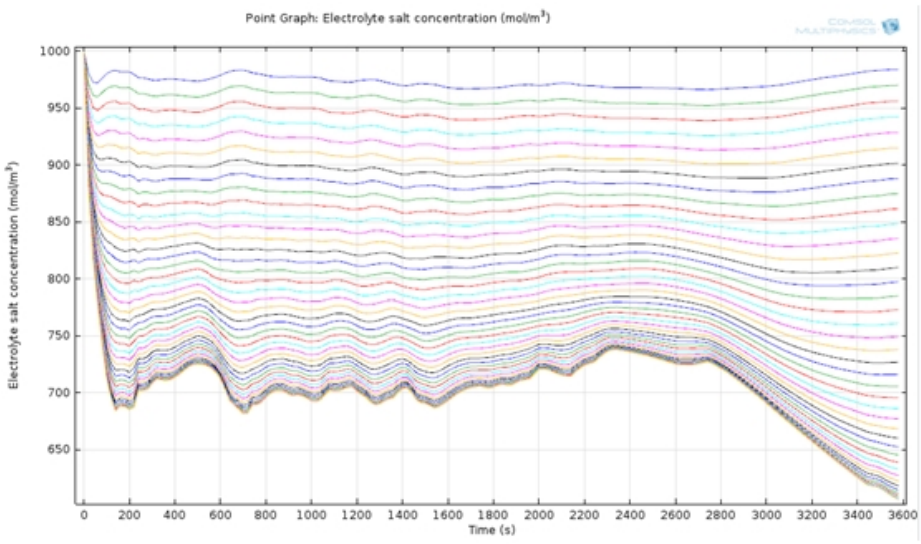

Figure 2.3. Electrolyte salt concentration during 1C discharge

For the same reason, Figure 2.3 can explain the phenomenon shon Figure 2.1(c). The curve of heat of mixing across electrolyte is correlated with the electrolyte salt concentration change.

Here we can know the trend and magnitude of heat of mixing, but to know how important it is, we need to compare it to other heat sources. Figure 2.4 is the powers for the different heat generations. It is obvious that the power of reversible heat is larger than the power of irreversible heat and heat of mixing.

To compare the heat power more clearly and directly, several time points were selected to show the ratio of the power of heat of mixing to the power of irreversible heat and the power of reversible heat. Table 2.2 shows the results of the percentage comparison of the powers. The power of heat of mixing is only 1 percent lower than the power of reversible heat in the most of the time. The highest value of the percentage to the total heat power is about 10 percent.

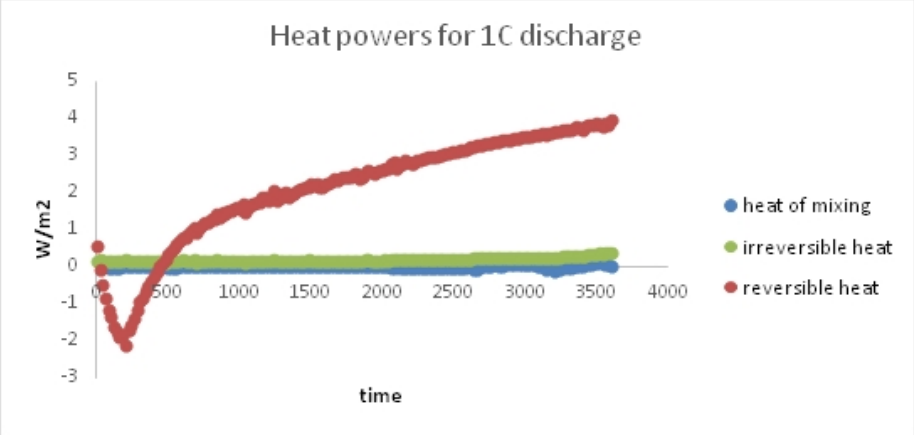

Figure 2.4. Powers of heat of mixing, reversible and irreversible heat in 1C discharge

Table 2.2. Percentage of power heat of mixing to other heat sources

Time	Heat of mixing	Irreversible heat	Reversible heat
300	-0.00022	0.13109 (-0.17%)	-0.96508 (0.03%)
500	-0.01788	0.15449 (-11.57%)	0.34901 (-5.12%)
2000	-0.01232	0.16692 (-0.74%)	2.62226 (0.47%)
3600	0.02663	0.39048 (6.82%)	3.956509 (0.67%)

Lastly, the total energy generation of the heat of mixing, irreversible heat and reversible are also simulated. The results are show in Figure 2.5. The heat of mixing is meaningful to be considered at the beginning of the discharging process, but can be neglected with the reversible heat quickly generated.

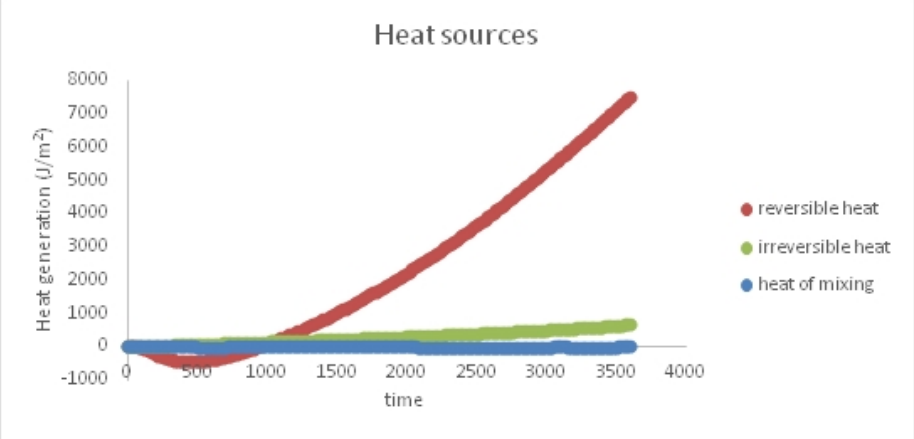

Figure 2.5. Energy generation of heat of mixing, reversible heat and irreversible heat in 1C discharge

2.1.2 Different C Rate

C rate has the most significant influence on the heat generation, so it is very necessary to first compare the heat of mixing generation at the different C rates. In the research, 0.1 C, 1 C and 5 C were applied for the simulation.

The 1 C rate simulation results have been shown in the previous standard model results. The enthalpy change across the electrode and electrolyte are necessary to be considered about. Compared to them, the enthalpy change within the particles is very small.

However, the situation is different when we applied the current density as 0.1 C and 5 C rate. For the 0.1 C, the results are shown below:

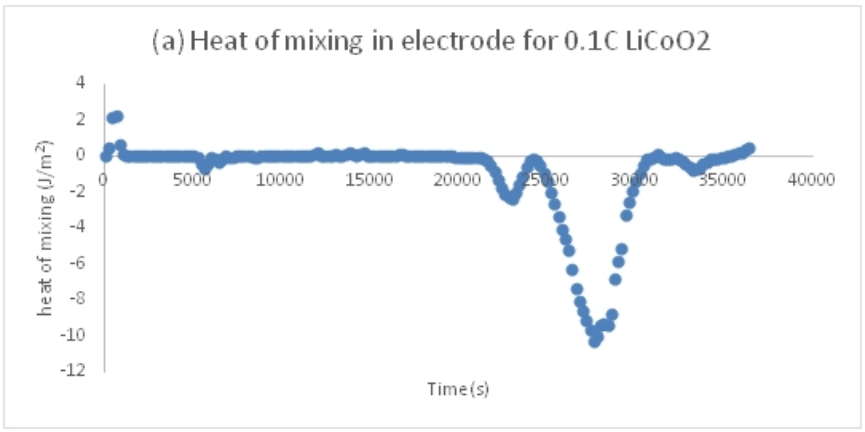

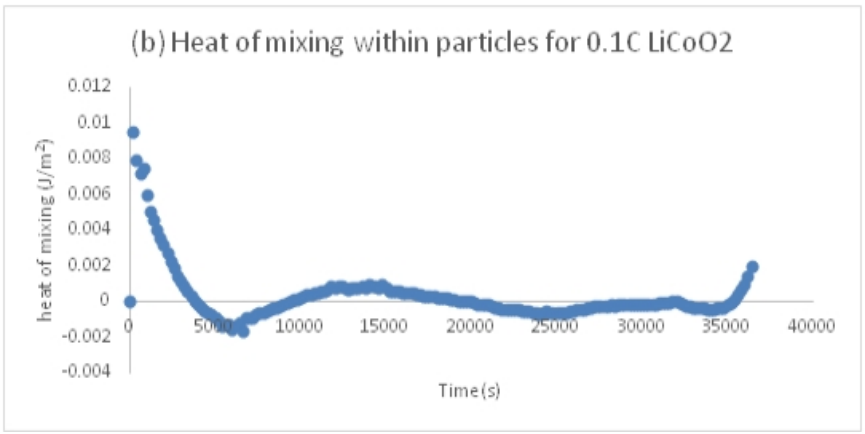

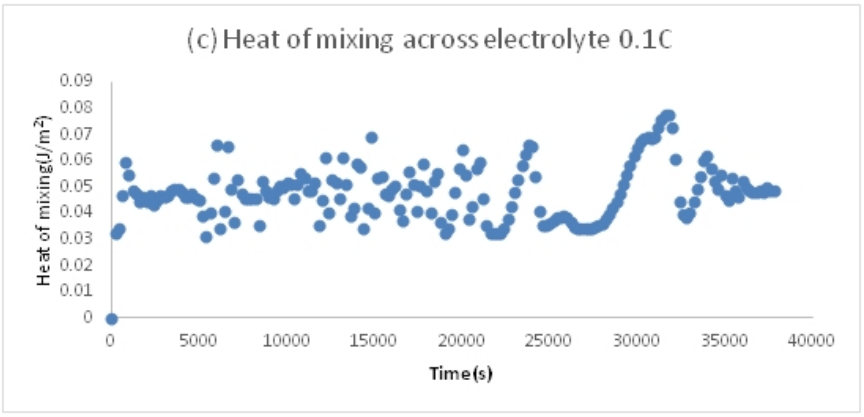

Figure 2.6. The heat of mixing for the 0.1C discharge

From the Figure 2.6(a) and Figure 2.6(b), the value of enthalpy change in electrode and the enthalpy change within particles are 5-10 times smaller than the results under the 1 C rate. The enthalpy change in electrolyte is not uniform like it is under the 1 C rate, which is because the electrolyte salt concentration change under 0.1 C rate is very small. The concentration goes up and down in a small range, so that the enthalpy change has a similar curve to it. Figure 2.7 shows the electrolyte salt concentration change in the cathode. It looks jumpy, but it is because the concentrations change is very small due to the low current density.

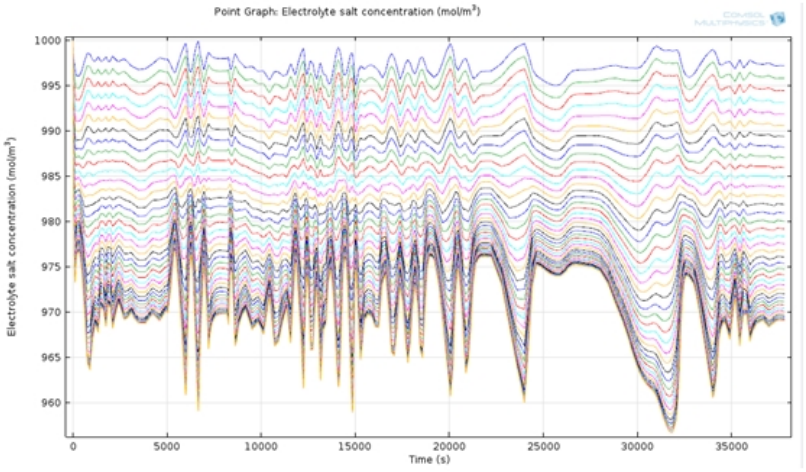

Figure 2.7. Electrolyte salt concentrations in 0.1C rate

In the next step, the heat of mixing generation under the 5 C rate was investigated. Because of the high current density, the discharging process cannot be finished, and it stopped at around 0.6 of state of discharge (SOD). To compare the results with the standard model of 1C rate, it was easy to see the difference of magnitude. Although the discharging process stopped quickly, the highest value of enthalpy change still got -200 J/m_2, which was 10 times larger than it was under the 1 C rate.

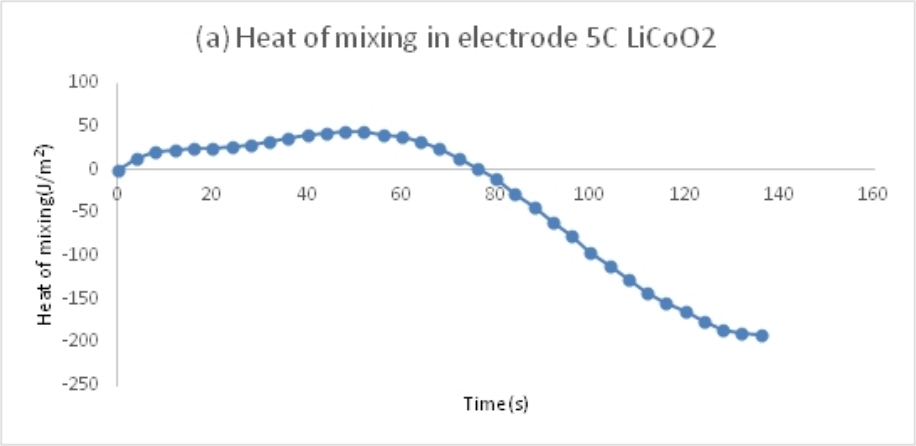

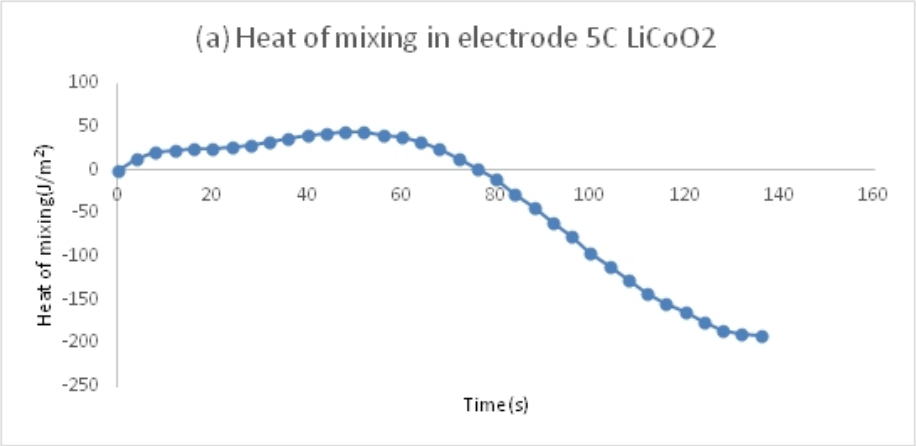

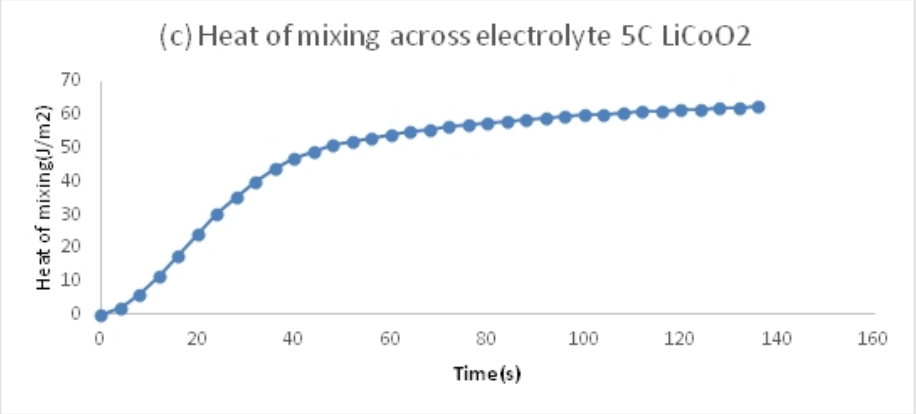

Figure 2.8. Heat of mixing for the 5C discharge

From the electrolyte salt concentration curve for the 5 C discharging process, we can find why it stopped early. Because the Li+ concentration reached the maximum value on the surface of the particles, the potential in the cathode went down very quickly. It led to the cell voltage decreasing and reaching the stop condition at 0.6 SOD. This phenomenon is based on the high diffusivity of electrolytes, which will be discussed in the next chapter in detail.

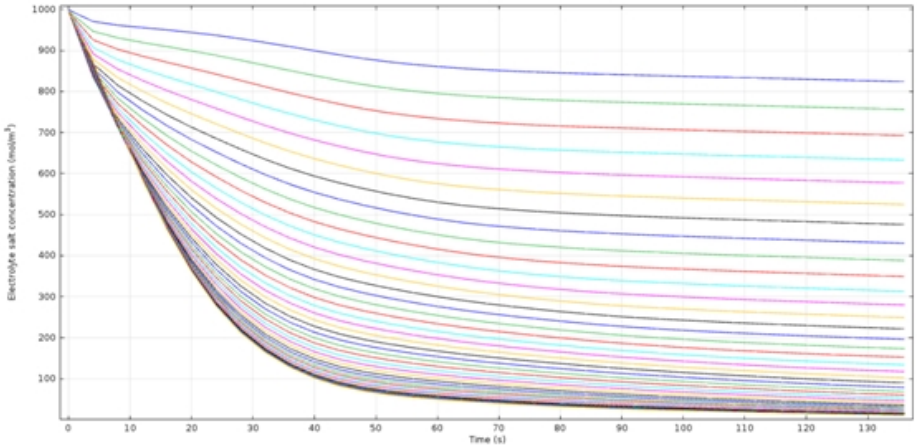

Figure 2.9. Electrolyte salt concentrations in 5C rate

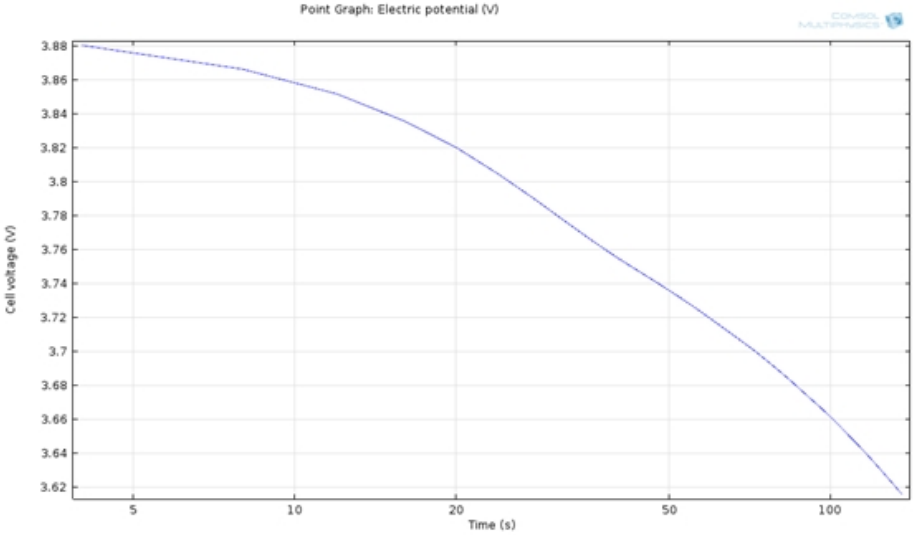

Figure 2.10. Cell voltage of 5C discharge

The stop condition for this simulation is cell voltage less than 3.6 V, so that the discharge process stops at 0.59 SOD. It is also why the Li ion batteries cannot be fully charged or discharged in high C rates.

2.1.3 Heat of Mixing in The Charging Process of Different C Rate

To think about the difference between the charging and discharging process, the heat of mixing generation during the charging process is shown below. The basic parameters for the simulation are the same, what changed was only current direction.

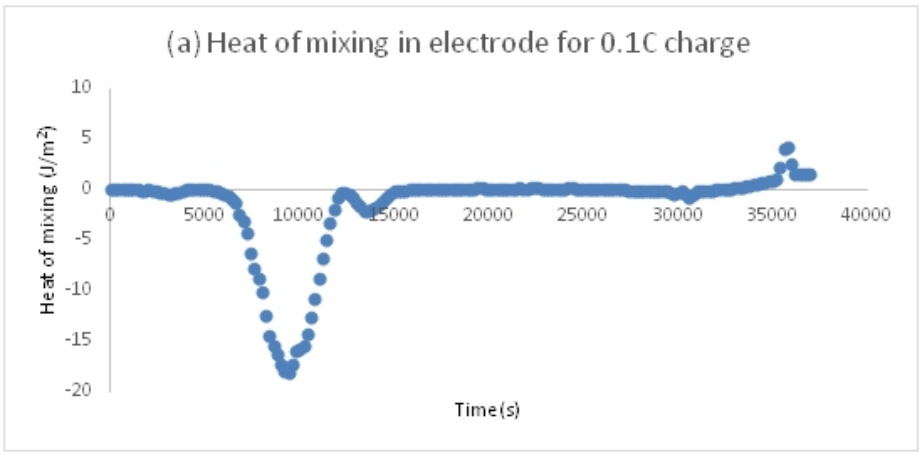

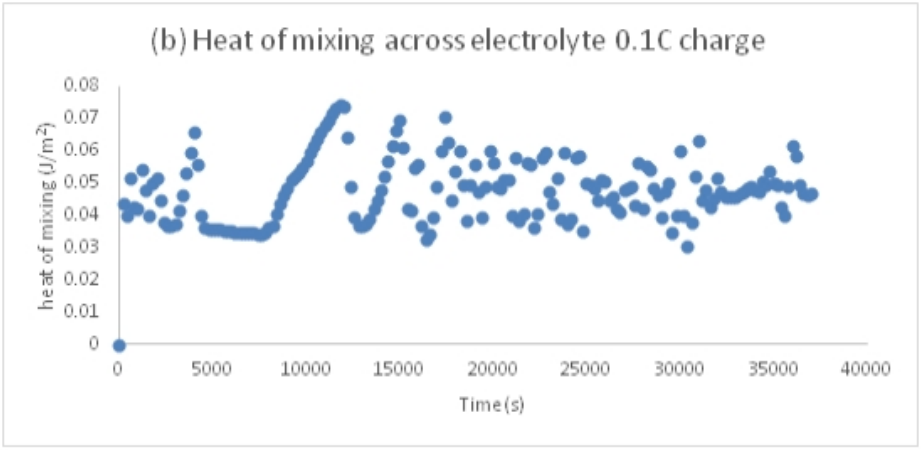

Figure 2.11. Heat of mixing for 0.1C charge process

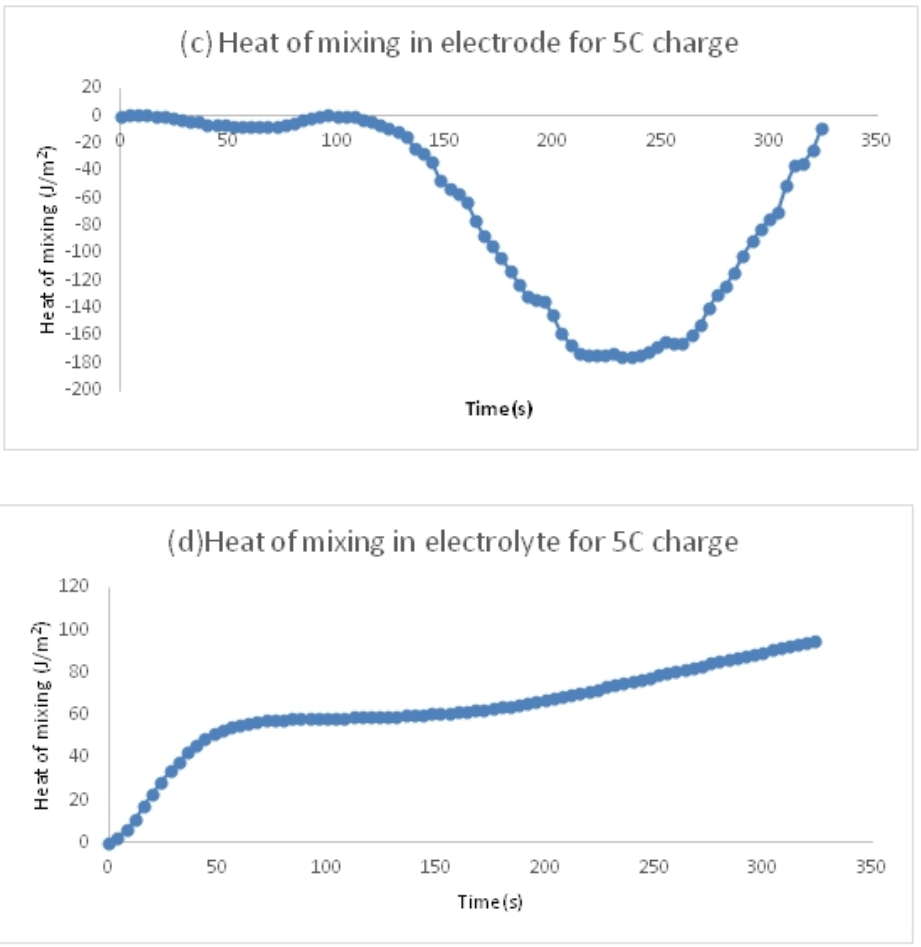

Figure 2.12. Heat of mixing for 5C charge process

The curves trend just like the opposite curves for the discharging process, so the explanation for the discharge curves can also explain the curves for charge.

Combined with the results from charging and discharging simulation, the conclusion is the heat of mixing doesnt make up a high percentage in the total heat generation, but it is more meaningful to consider under the high C rate charge or discharge.

2.1.4 Different Particle Sizes

Particle size of anode and cathode material is directly related to the lithium ion diffusion path length, which has a huge impact on electrodes performance at the high rate [14]. When the particle size is small and specific surface area generally large, on the one hand, it can make the current density of the electrode decrease to reduce the polarization of the working electrode; on the other hand, it can provide more channels for lithium ion transport and shorten the migration path, reducing diffusion impedance, thereby improving the high-rate performance of electrodes. Therefore, the material that has smaller particle sizes and nanostructures (nanospheres, nanowires, nanorods, nanotubes and nano-film) typically exhibits better performance than the lithium-ion battery cathode materials [3].

Particle size of a spherical object equals to its diameter. Here, it is presented by radius. The heat generation can be influenced by particles sizes. In the standard model, which was shown previously, the particle radius was 2 μm. To compare with the standard results, 1 μm radius and 4 μm radius were taken. The simulation results are shown below:

The difference of heat of mixing for the different particle size is mainly in electrodes. The curves of heat of mixing across the electrolyte are almost same. The difference comes from inside the particle. Because the particle diameter decreases, the concentration gradients become smaller, so the heat of mixing within a single particle should reduce. However, because the concentration gradients were small, it is not a big difference for a single particle, but the number of particle in the same volume will increase dramatically. This leads to the heat of mixing within particles increasing.

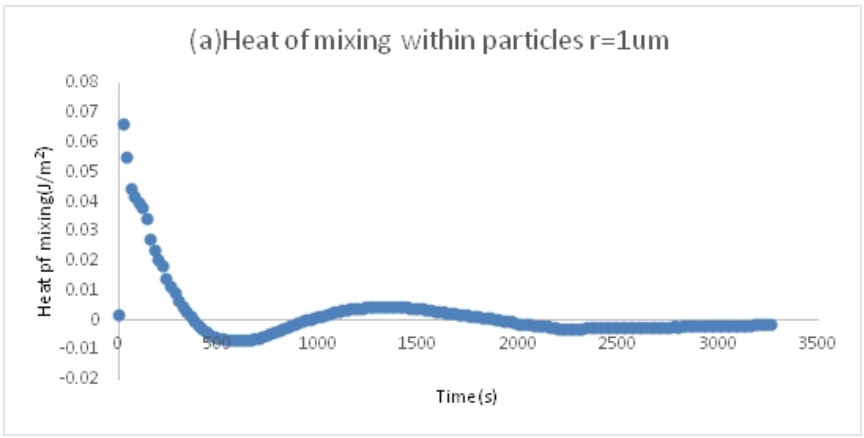

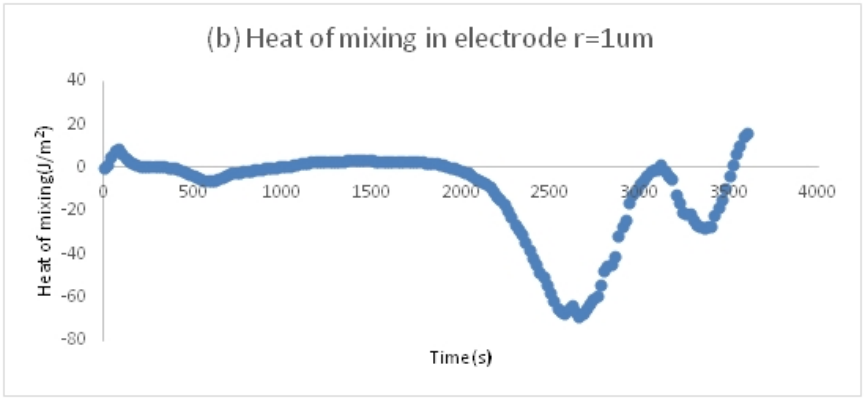

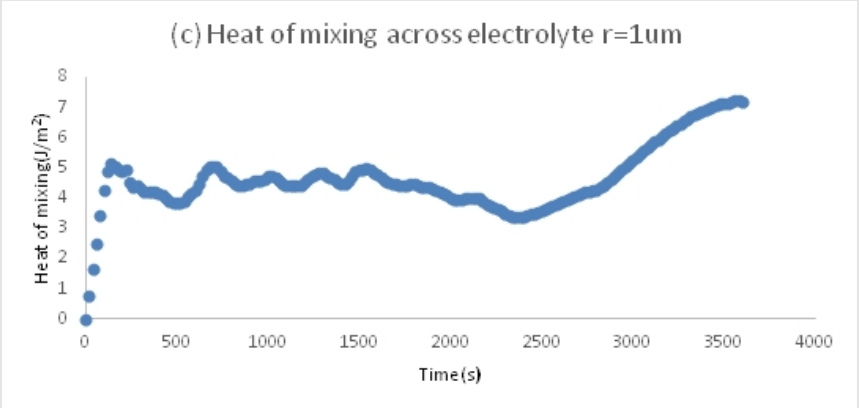

Figure 2.13. Heat of mixing for the particle size r = 1 μm

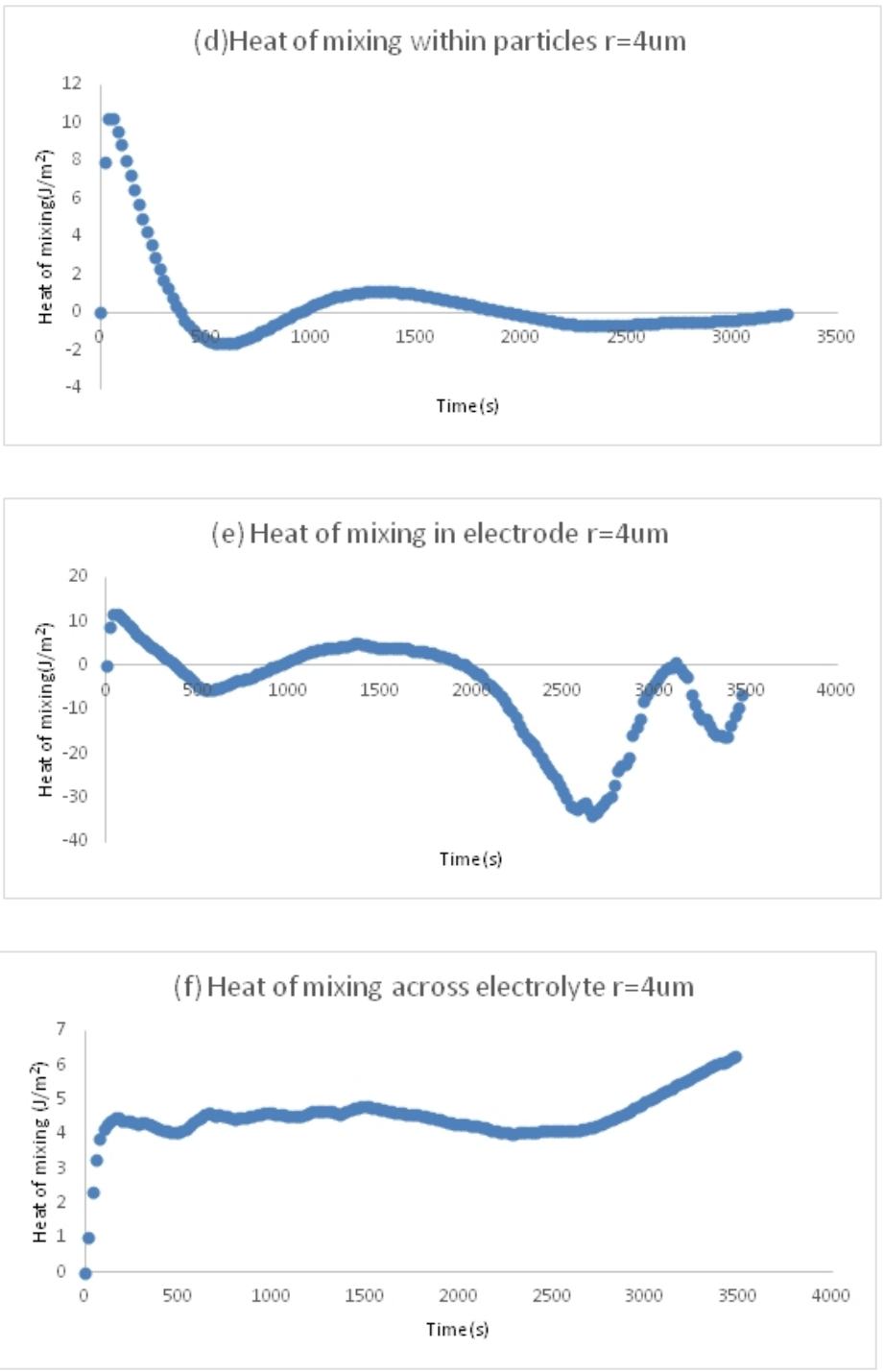

Figure 2.14. Heat of mixing for the particle size r = 4 μm

2.1.5 Different Porosity

Porosity is a measure of the void spaces in a material, and is a fraction of the volume of voids over the total volume, between 0 and 1, or as a percentage between 0 and 100 percent. There are many ways to test porosity in a substance or part, such as industrial CT scanning. The term porosity is used in multiple fields including pharmaceutics, ceramics, metallurgy, materials, manufacturing, earth sciences, soil mechanics and engineering.

Generally, the porosity is presented as the function below:

$$\varepsilon = \frac{\mathrm{V_V}}{\mathrm{V_T}} \tag{2.1}$$

where V_V is the volume of void space and V_T is the total or bulk volume of material, including the solid and void components. Apply different pressures during the electrode production process, can yield different porosity of the material. In the standard model, we assumed that the porosity equals 0.3 as ideal condition. In this part, to investigate the influence of different porosity to the heat of mixing, 0.4 and 0.5 were applied to simulate heat of mixing.

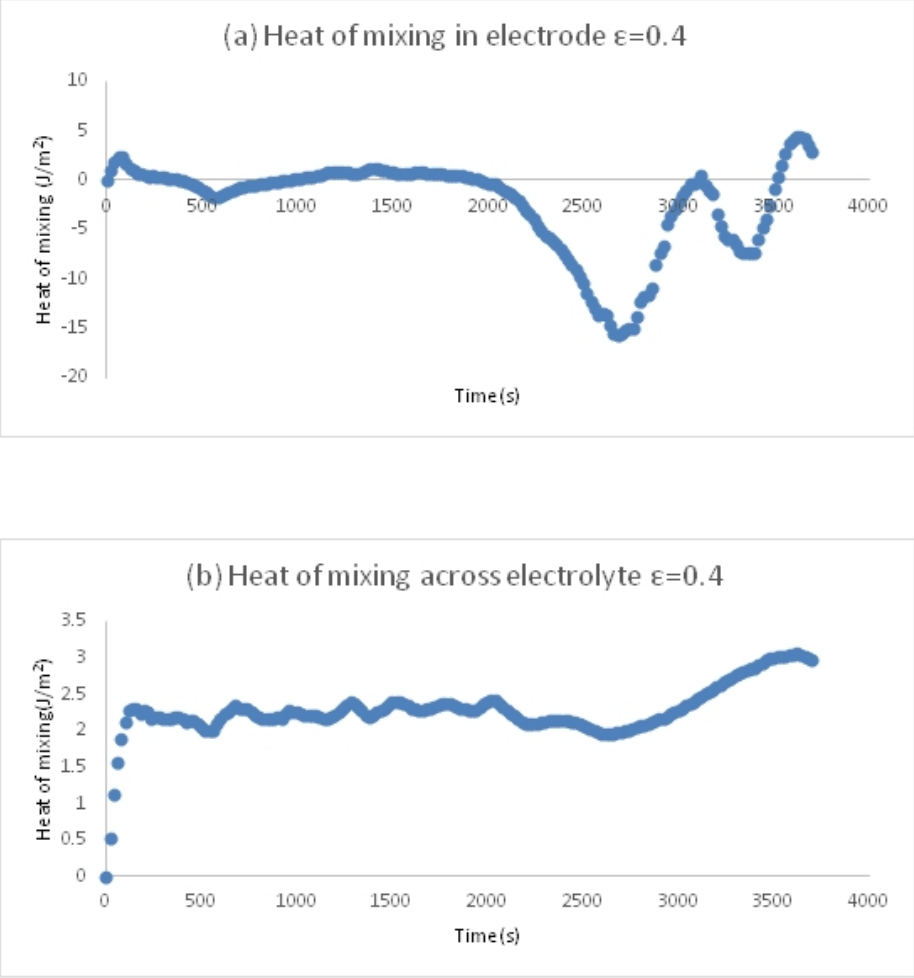

Figure 2.15. Heat of mixing for the porosity equal to 0.4

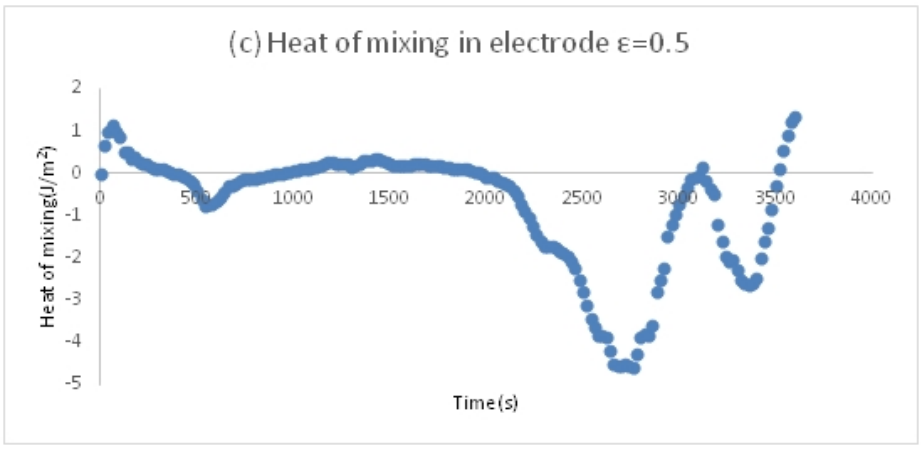

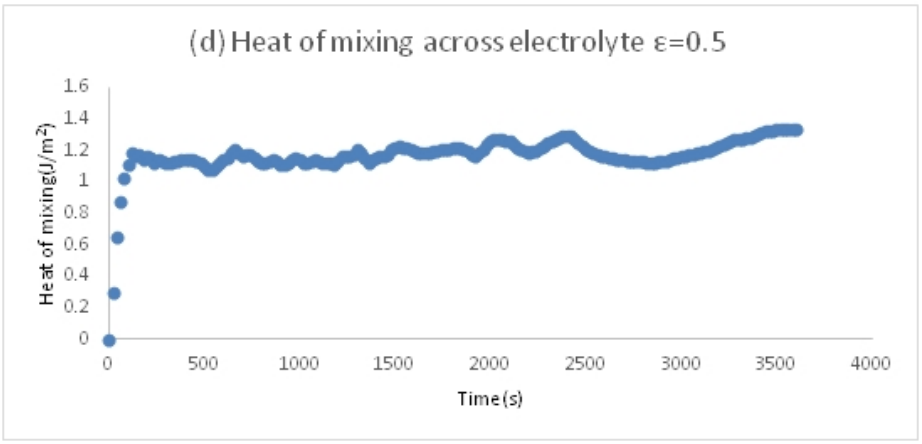

Figure 2.16. Heat of mixing for the porosity equal to 0.5

From Figure 2.15 and Figure 2.16, we can see that the heat of mixing is higher in the electrode with lower porosity obviously. It is because the electrode with low porosity has more active materials and the higher Li ion concentration gradient in electrolyte at low porosity. The electrode has higher porosity means electrolyte can go through it easier, so that the concentration gradient in electrolyte it lower than it is in the electrode with smaller porosity. That is the reason of heat of mixing across electrolyte with small porosity is larger than it is in high porosity electrode.

2.1.6 Different Thickness

The thickness of the electrode can be changed, so we can make different thickness of the material. In this simulation, 50 μm, 70 μm, and 90μm were applied as the thickness.

The active material increases with the thickness increase. Therefore, the heat of mixing have to be increased too. However, from figures, we found the heat of mixing increased with the electrode thickness dramatically. It is because the current density increased for the thicker electrode. To charge a battery with thicker electrode to full, higher current needs to be applied for extra active material. Then, the higher current lead to the larger concentration gradient and faster change.

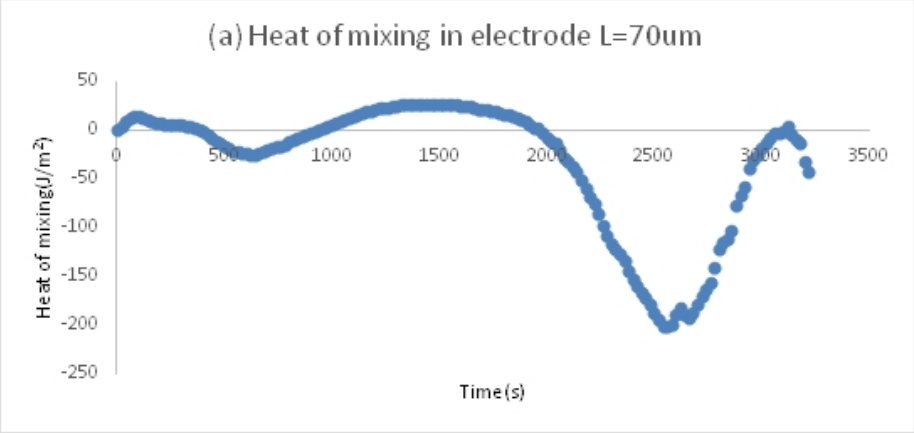

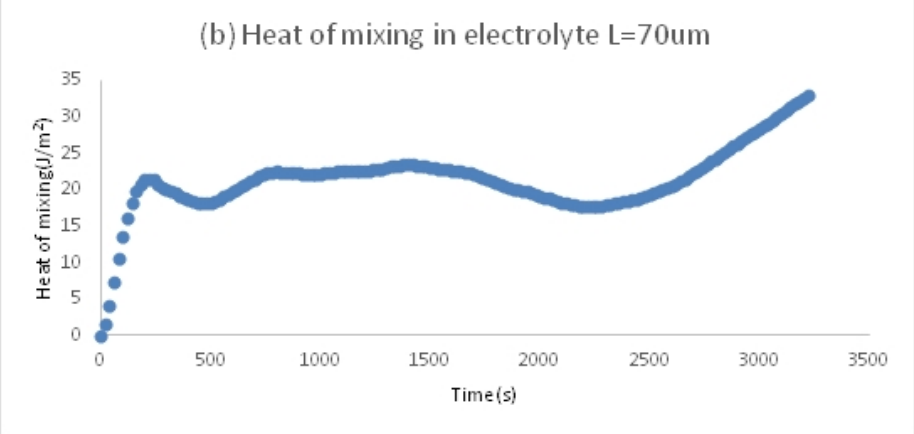

Figure 2.17. Heat of mixing for the thickness equal to 70 μm

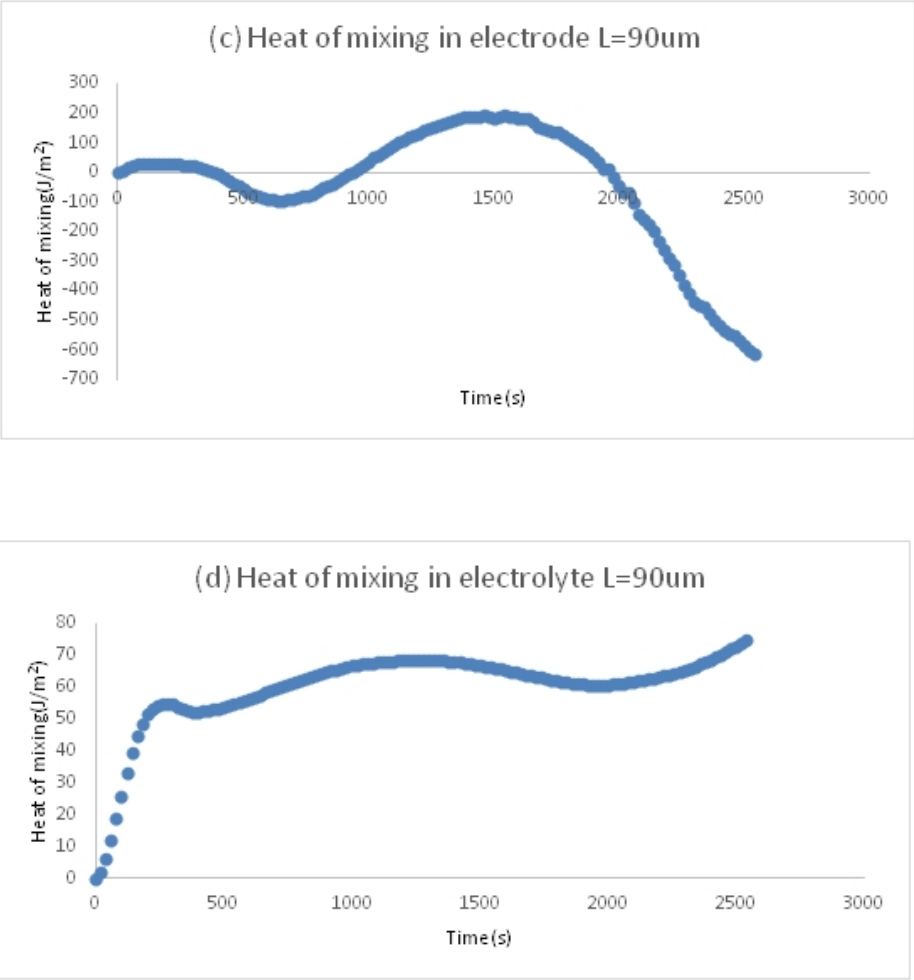

Figure 2.18. Heat of mixing for the thickness equal to 90 μm

2.2 Investigation on LiC_6

Synthetic graphites, such as mesocarbon-microbead (MCMB) have been used commercially by many battery companies as anode materials in LIBs because they have shown a reversible electrochemical behavior and a low, flat potential curve for the lithium intercalation/deintercalation process. LiC_6 is the most commonly used for the anode electrode of LIBs. It has high power density and flat potential curve.

In the full cell model, it is meaningful to consider the heat generation from both electrodes. Actually, in most situations, the heat of mixing in the anode is larger than the heat of mixing in the cathode.

The basic parameters of the anode are shown in Table 1.1 and Table 2.1. The heat of mixing was calculated with the same method as $LiCoO_2$, so the derivative of partial molar enthalpy over concentration obtained by equation (3) and (4) of LiC_6 needs to be applied.

2.2.1 Different C Rate

In the research, the heat of mixing in the anode for the different C rates was simulated to compare to the cathode materials. Just as it in the cathode simulation, 0.1 C, 1 C and 5 C were applied.

Standard model for 1 C rate:

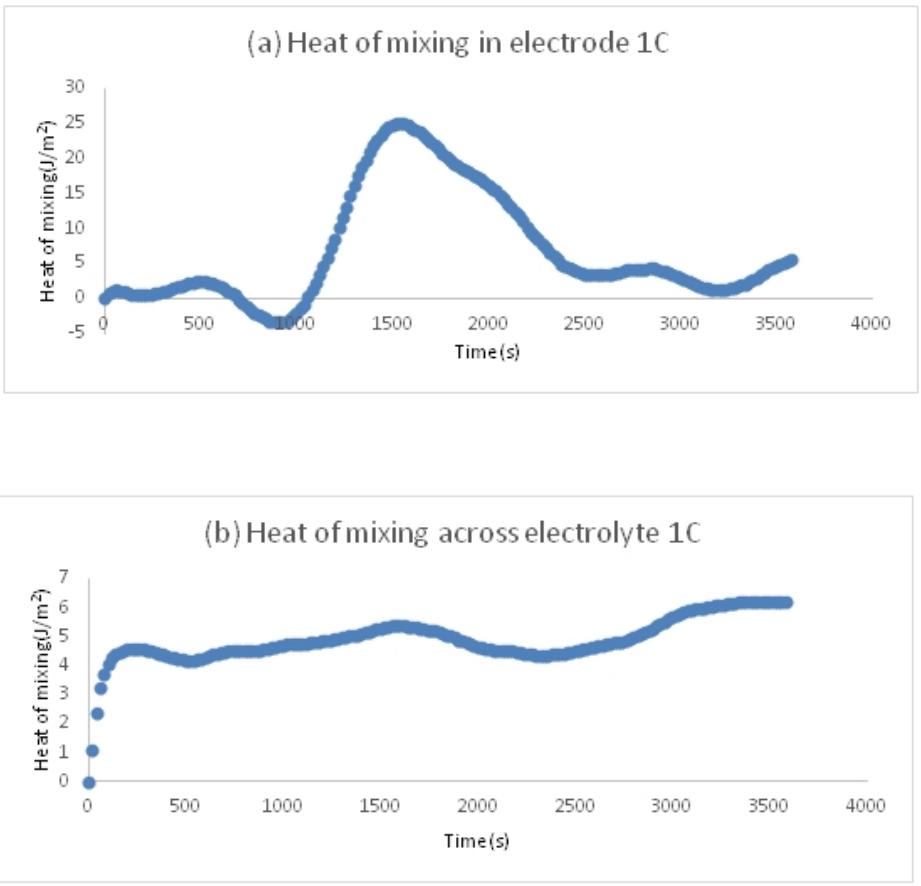

Figure 2.19. Heat of mixing at 1C rate for anode

Figure 2.19 shows the standard model results for LiC_6 anode. Because of the larger particle size, the heat of mixing within particles is larger than in the cathode. Also, the concentration gradient is larger than the gradient in the cathode due to the smaller diffusivity.

Figure 2.20 shows the concentration across the electrode in the anode. The legend shows the elements in the electrode. There is no big jump or drop during the process. Thats why it has smaller heat of mixing.

Above are the heat of mixing results for the different C rates. For the same reason that discussed in 0.1 C results, the heat of mixing across the electrolyte is still not uniform due to the tiny change of the electrolyte salt concentration. The process for

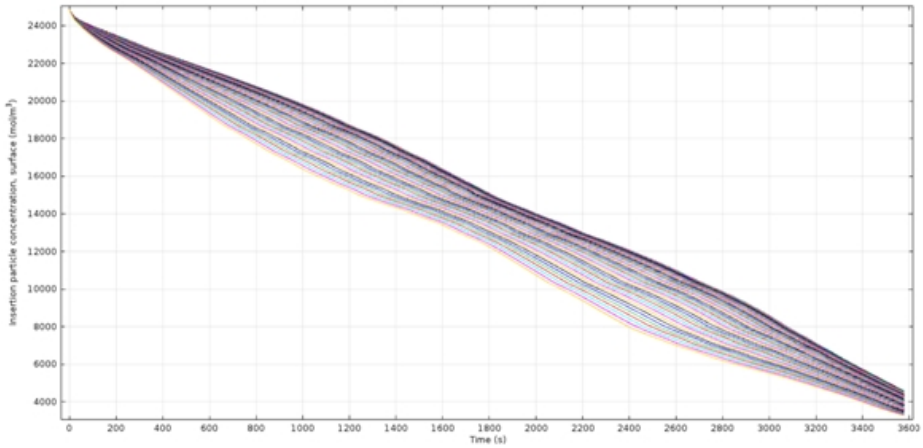

Figure 2.20. Li ion concentration change along the electrode

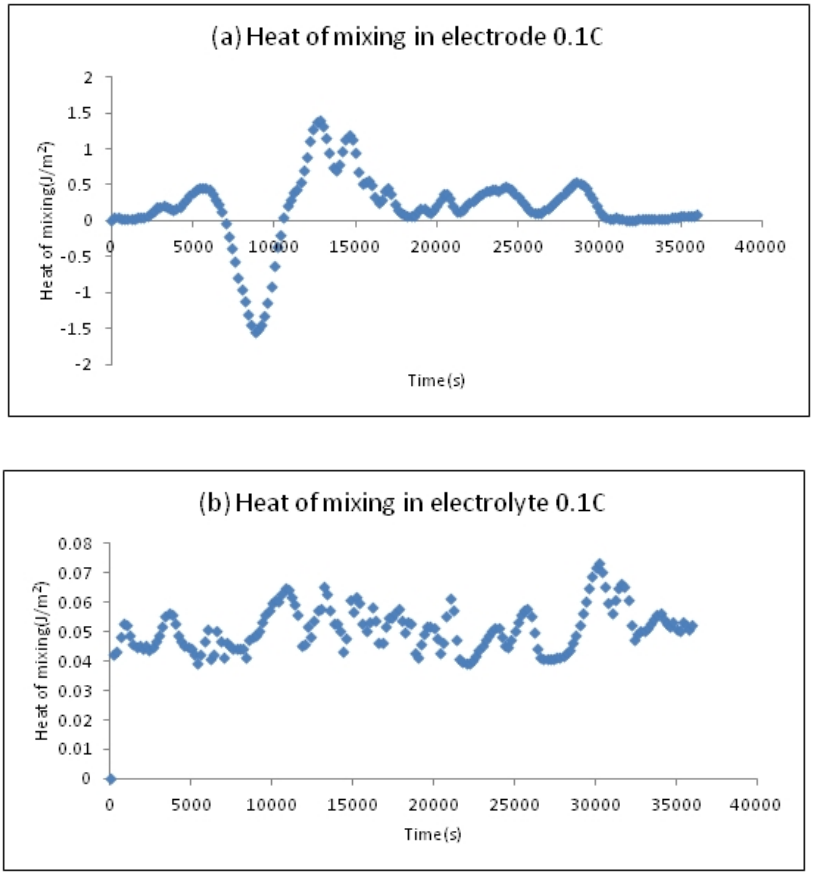

Figure 2.21. Heat of mixing at 0.1C rate for anode

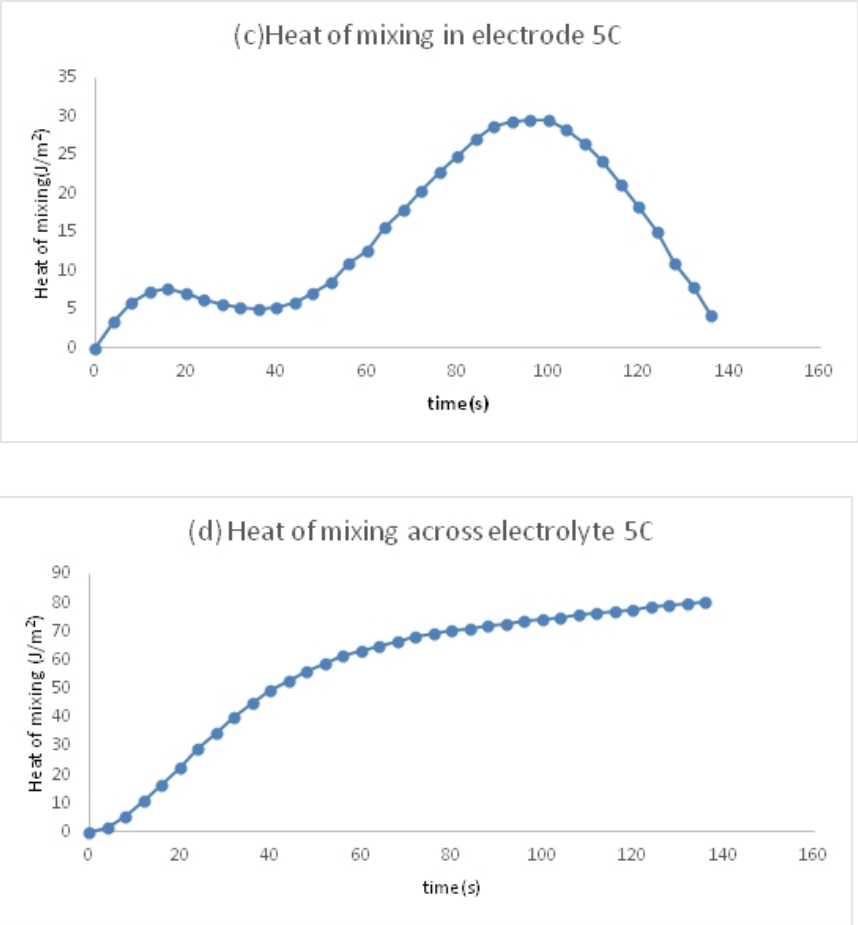

Figure 2.22. Heat of mixing at different 5C rate for anode

5 C stopped early due to the cell voltage decreasing quickly, so that we cannot see the maximum value for this process, but it will be shown later.

2.2.2 Different Anode Particle Sizes

Because the results of cathode material simulation showed that the particle size influences the heat of mixing, the same simulation was done for the anode. In the standard model, we applied 7.5 μm as the radius, and used 6 μm and 9 μm radius to compare with it. The heat of mixing curves of r = 7.5 μm are the same as those shown in the standard model results. The curves of heat of mixing for r = 6 μm and 9 μm are showed in Figure 2.23 and Figure 2.24.

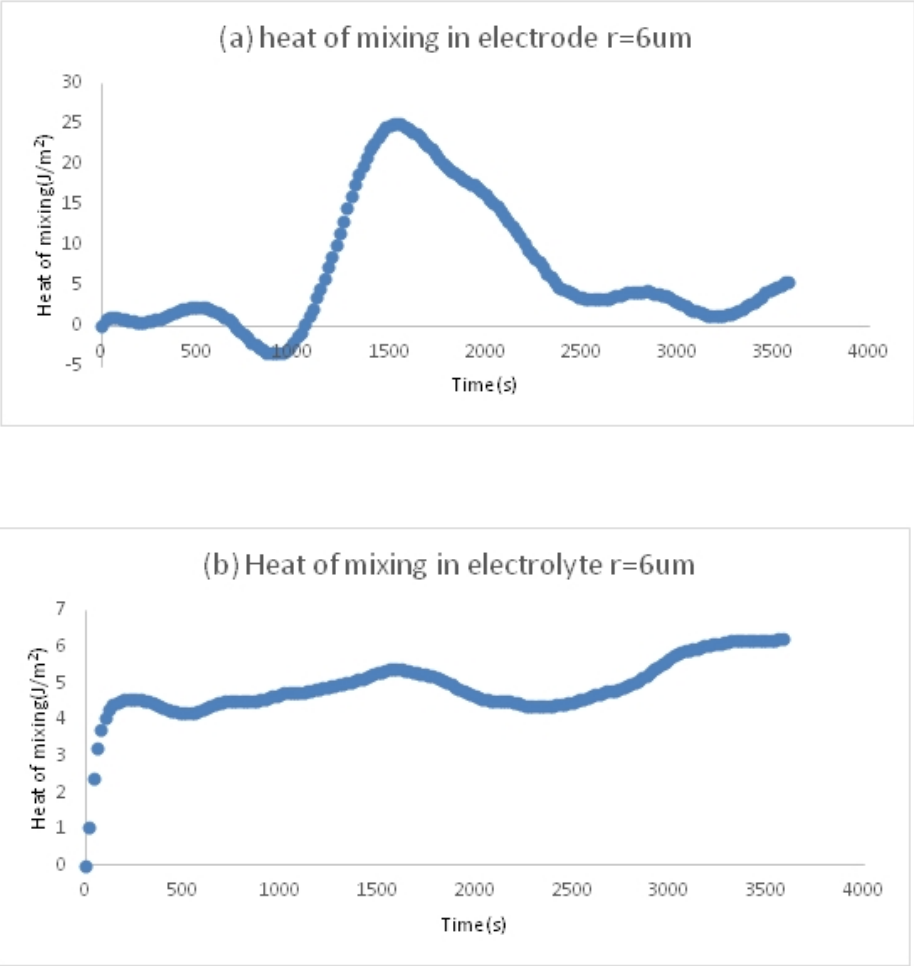

Figure 2.23. Heat of mixing for the radius of particle in anode equal to 6μm

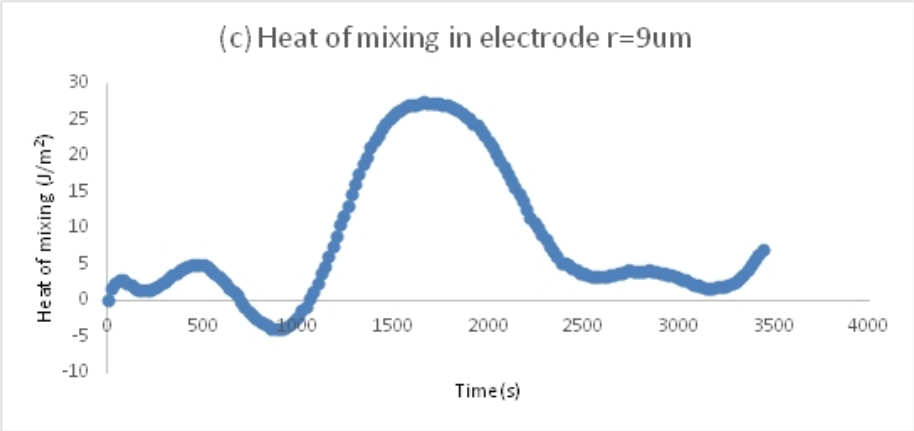

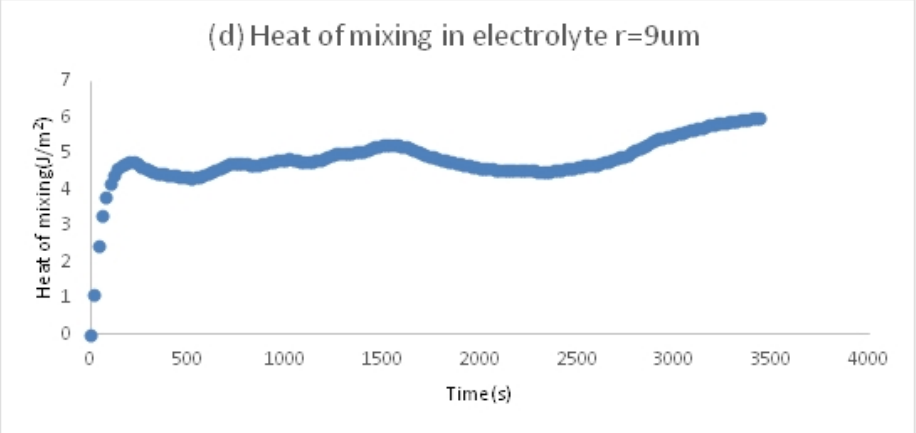

Figure 2.24. Heat of mixing for the radius of particle in anode equal to 9μm

2.3 Investigation on $LiMn_2O_4$

As reference, another cathode material was also investigated the heat of mixing in cathode electrode. Different parameters were applied, especially to the diffusivity.

2.3.1 Standard Model

Table 2.3. Parameter of the $LiMn_2O_4$ standard discharge model

Name	Value	Description
i_1C	15.6 [A/m^2]	1C discharge current
Ds_neg	2.52e-14[m^2/s]	Solid phase Li-diffusivity Negative
Ds_pos	1e-14[m^2/s]	Solid phase Li-diffusivity Positive
rp_neg	6e-6[m]	Particle radius Negative
rp_pos	1e-6[m]	Particle radius Positive
T	298 K	Temperature
Dl	7.5e-11[m^2/s]	Salt diffusivity in Electrolyte
epsl_pos	0.3	Electrolyte phase vol-fraction Positive
epss_pos	0.7	Solid phase vol-fraction Positive
cl_0	1000[mol/m^3]	Initial electrolyte salt concentration
epsl_neg	0.3	Electrolyte phase vol-fraction Negative
epss_neg	0.7	Solid phase vol-fraction Negative
csmax_neg	31858[mol/ m^3]	Max solid phase concentration Negative
csmax_pos	23700[mol/ m^3]	Max solid phase concentration Positive
cs0_neg	csmax_neg*0.78	Initial Negative State of Charge
cs0_pos	csmax_pos*0.25	Initial Positive State of Charge
L_neg	45e-6[m]	Length of negative electrode
L_sep	15e-6[m]	Length of separator
L_pos	50e-6[m]	Length of positive electrode

Lithium manganese oxides theoretical specific capacity is 283 mAh/g, and the actual specific capacity is between 110 to 120 mAh/g. Its advantage is good stability,

non-polluting, high voltage, and low cost. Currently the applications are mostly $LiMn_2O_4$ in Spinel type, having a three-dimensional tunnel structure. The average operating voltage of $LiMn_2O_4$ is about 3.8V.

Standard model results:

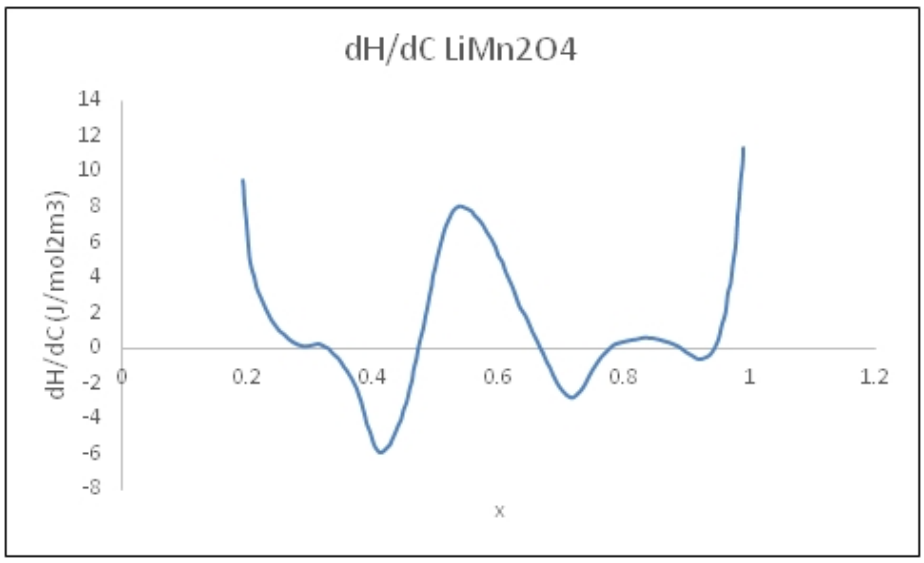

Figure 2.25. The derivative of partial molar enthalpy over concentration of $LiMn_2O_4$

To simulate the heat of mixing for $LiMn_2O_4$, the derivative of partial molar enthalpy over concentration of $LiMn_2O_4$ also needs to know. Figure 2.26 is the dH/dC that we get from Zhangs paper. It was obtained by Equation (1.3) and (1.4) and based on the curve fit by entropy of $LiMn_2O_4$.

Figure 2.25 shows the results for the $LiMn_2O_4$ at 1C rate discharge. The maxmium value of the heat of mixing across the electrode is larger than the heat of mixing across the electrode in $LiCoO_2$, which is because the value of dH/dC is larger than dH/dC of $LiCoO_2$. The drop at the beginning of the curve of heat of mixing in the electrode is because of the large concentration gradient at that time. The concentration status is shown in Figure 2.26. Because the concentration gradient is so small at the medium period, the heat of mixing is also small during that period, although the dH/dC reaches the peak value at that time.

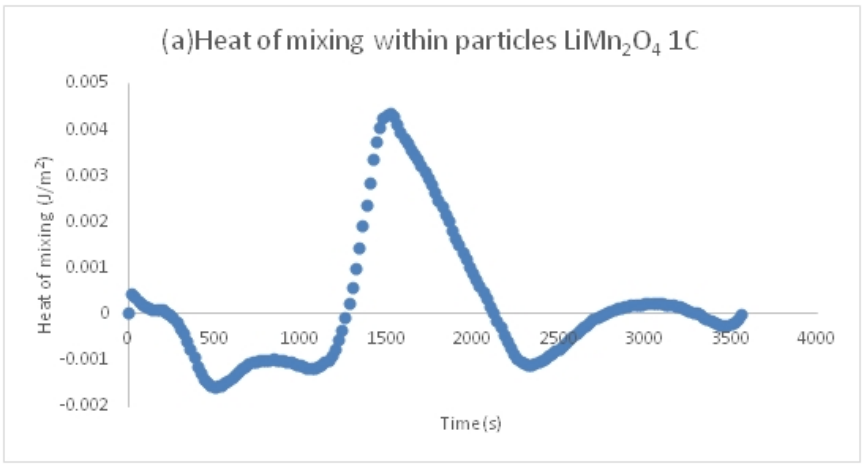

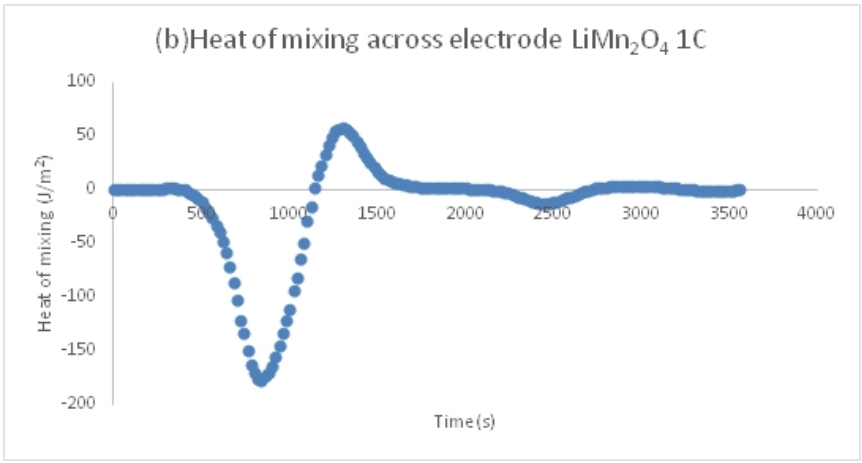

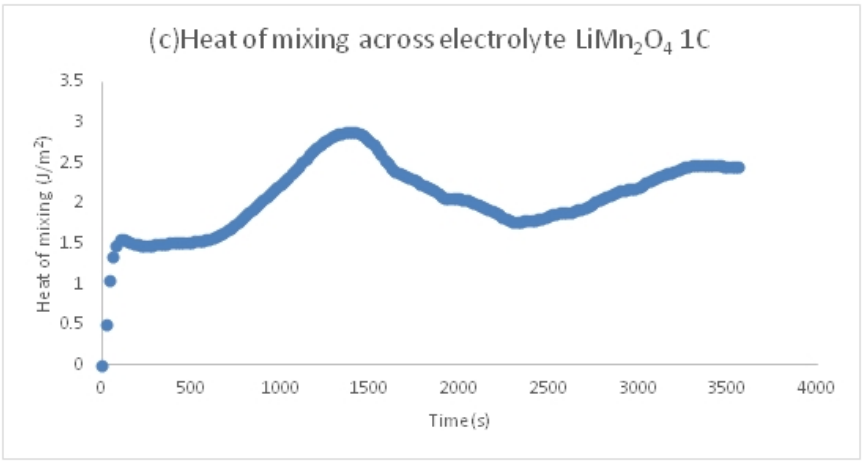

Figure 2.26. Standard model results of heat of mixing for $LiMn_2O_4$

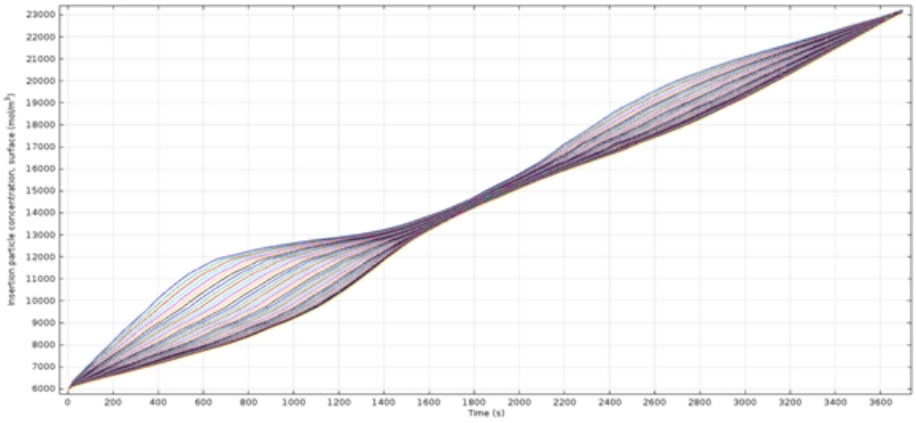

Figure 2.27. The Li ion concentration change along the $LiMn_2O_4$ electrode

2.3.2 Different C Rates

For the 0.1C rate, the heat of mixing across the electrolyte is also small enough to be ignored. The magnitude is the same as the magnitude of the results of 0.1C rate for $LiCoO_2$.

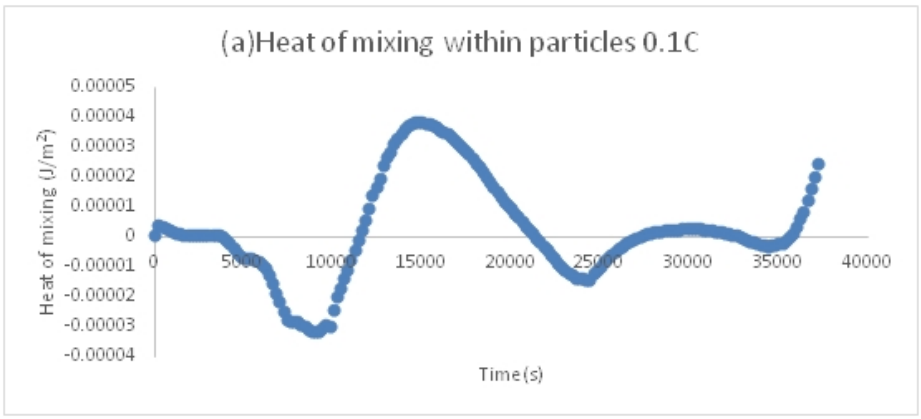

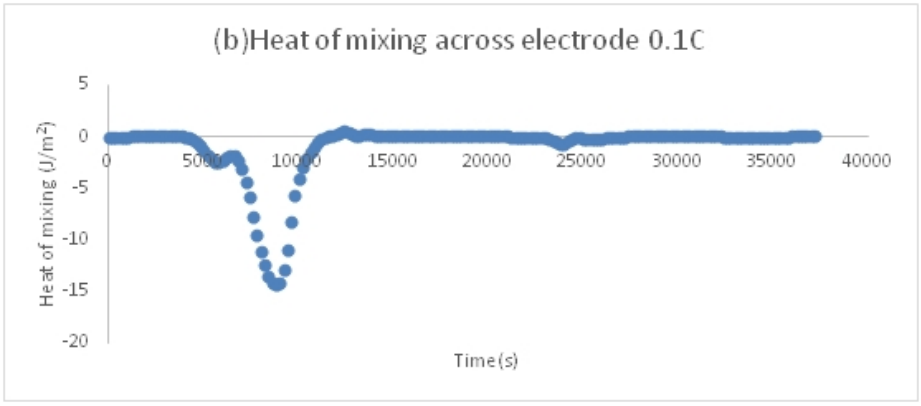

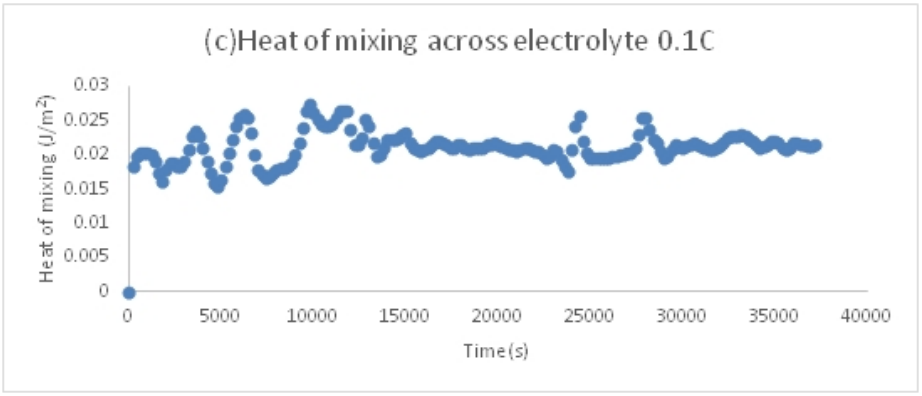

Figure 2.28. Heat of mixing at 0.1C rate for $LiMn_2O_4$

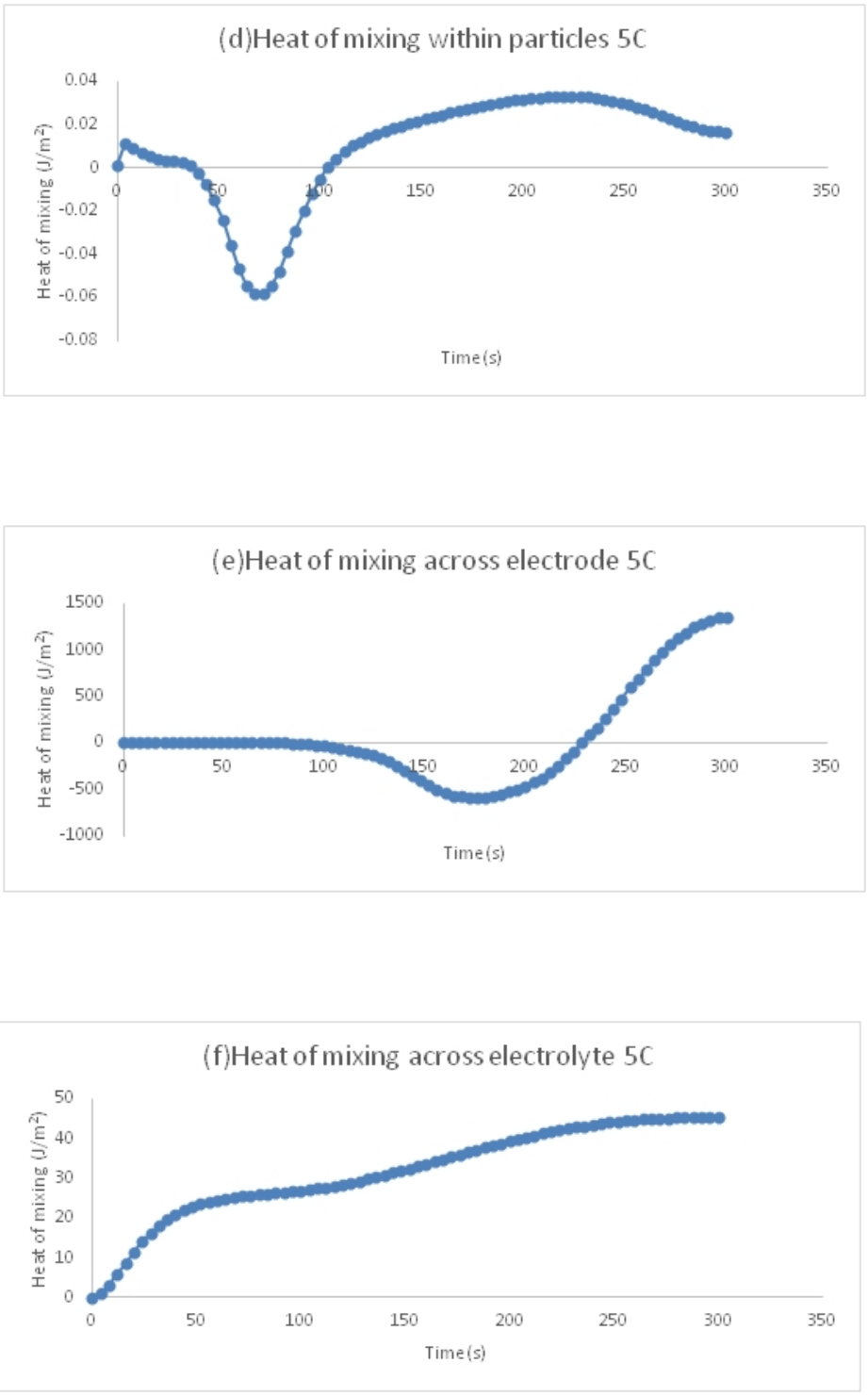

Figure 2.29. Heat of mixing at 5C rate for $LiMn_2O_4$

2.3.3 Different Particle Size

The particle size of $LiMn_2O_4$ is smaller than the particle size of $LiCoO_2$. Usually it is only a half of that. Therefore, to investigate the influence of particle sizes on the two materials, 0.5 μm, 1 μm and 2 μm were selected as the particle radius of $LiMn_2O_4$.

It is interesting that we found for the same particle size, such as r = 1 μm, the heat of mixing within particles of $LiCoO_2$ and $LiMn_2O_4$ has the same magnitude, but when the radius change to 0.5 μm for $LiMn_2O_4$, the heat of mixing within particles decreases dramatically. It is because the Li ion can reach the center of particle much easier within the smaller particles. Due to the shorter distance and the same diffusivity, Li ions take short time to reach the center after they get into the particles through surface. This phenomenon leads to the concentration gradient is smaller within smaller particles. Based on Equation (2), we can explain why the heat of mixing within particles changes dramatically with the particle size.

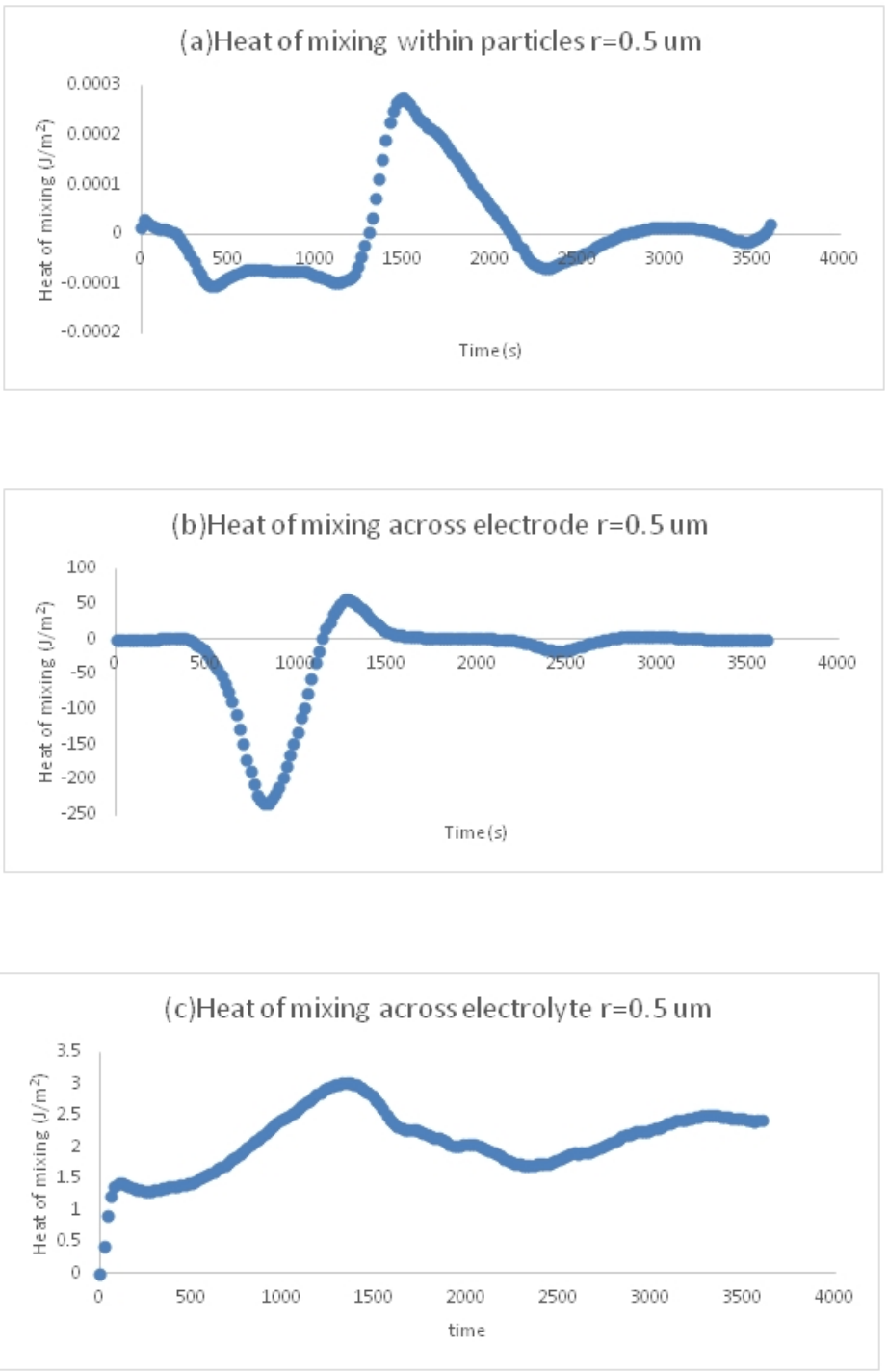

Figure 2.30. Heat of mixing for particle radius equal to 0.5 μm in $LiMn_2O_4$

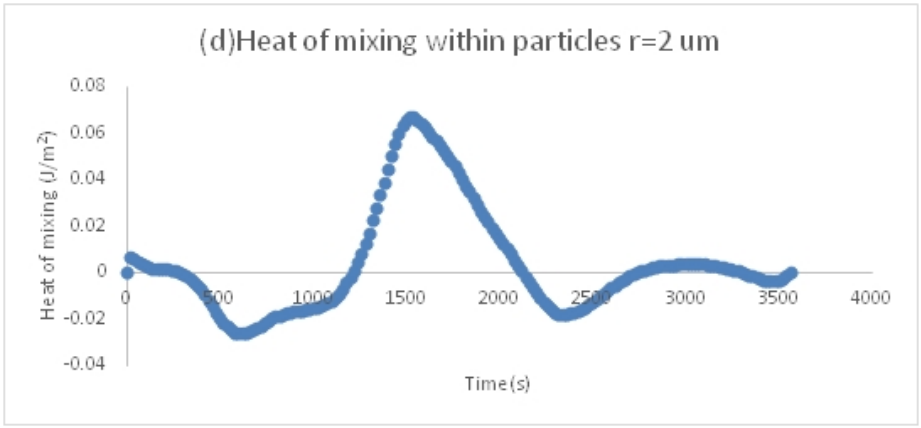

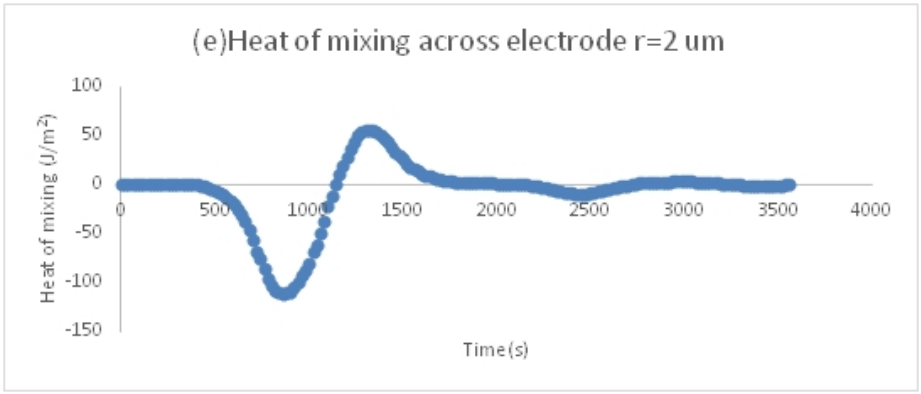

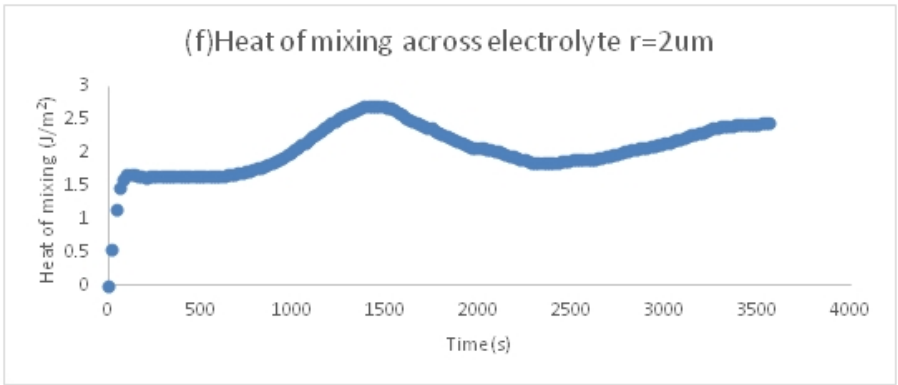

Figure 2.31. Heat of mixing for particle radius equal to 2 μm in $LiMn_2O_4$

2.4 Summary

From the above data, heat of mixing is influenced by C rate, particle size, porosity, and thickness. These are the parameters we can control during the manufacturing procedure and charging or discharging process. To summarize the results, heat of mixing not only increases with C rate and thicknesss increasing, but also increase with particle size and porositys decreasing. Based on these simulations, we can know how to control the heat of mixing change when it is necessary.

Another factor that should be noticed is the volume change. The volume expansion of the negative active material is 14 percent from C_6 to LiC_6 after fully charging [18], and the volume contraction of the positive active material is 1.07 percent from $Li_{0.4}CoO_2$ to $Li_{0.95}CoO_2$ after discharging [19]. If the particle volume changed, the concentration within particle will also change with it. The heat of mixing is significantly influenced by concentration gradient, so the volume change also has influence to the heat of mixing. The volume change was not discussed in this model is because the volume change in $LiCoO_2$ and LiC_6 is small. Even for $LiMn_2O_4$, the volume change is only 6.5 percent [20]. The influence to the concentration is not as important as the C rate and particle size. However, if Silicon is applied as the anode material, the volume change will be very important to consider. The volume change of silicon could reach 300 - 400 percent during cycling [21], so that the concentration will change dramatically with the volume change, and it will also be a significant factor of the heat of mixing.

In the comparison of heat of mixing and total heat, heat of mixing is quite small. It is usually lower than 10 percent of the total heat, sometimes even lower than 1 percent. Therefore, heat of mixing is not as important as resistive heat or reaction heat, but it is important to consider it when the other heat sources are also small.

Moreover, the heat of mixing is caused by concentration gradient, so it does not rely on external potential and current. It still exists after the charging or discharging process has been stopped. In that case, it has to be considered.

3. NANO CT EXPERIMENT

Many mathematical approaches of the previous section are based on using a homogeneous porous electrode with spherical particles. Those models assume a constant as the porosity, and calculate without the consideration of the pores construction. Actually, by using material properties and assumed geometrical characteristics, the models successfully described most of electrochemical performance of LIBs. However, the homogeneous electrode models were found to analyze material degradation and localize particle interactions for LIBs without morphological effects [22]. The effects will eventually influence the LIBs voltage specific capacity, and discharge/charge rate due to the electron and lithium ions transportation. Therefore, it is important to develop the realistic 3D geometry of the electrode material to enhance the transport simulations and degradation predictions. X-ray computed tomography (CT) is the method that was chosen to build the 3D geometry. It is a technique that enables the reconstruction of the 3D morphology.

The goal of this research:

- Quantify geometric characteristics of a porous electrode
- Reconstruct anode electrode using x-ray micro- and nona-CT
- Quantify porosity, specific surface area, tortuosity, pore size distribution

In this section, a synchrotron X-ray CT technique will be used to understand 3D miscrostructure acquisition of LIB electrodes.[19, 20] It is a non-destructive tomographic method without physical sectioning and epoxy filling. Therefore, it allows continuous morphological evolution studies of the porous materials with a high spatial resolution and good image contrast. In the experiment, the electrode was broke into some tiny pieces. One of the pieces was selected due to the uniform edges and great top angle to view.

A schematic of the Nano-CT configuration is depicted in Figure 3.1.

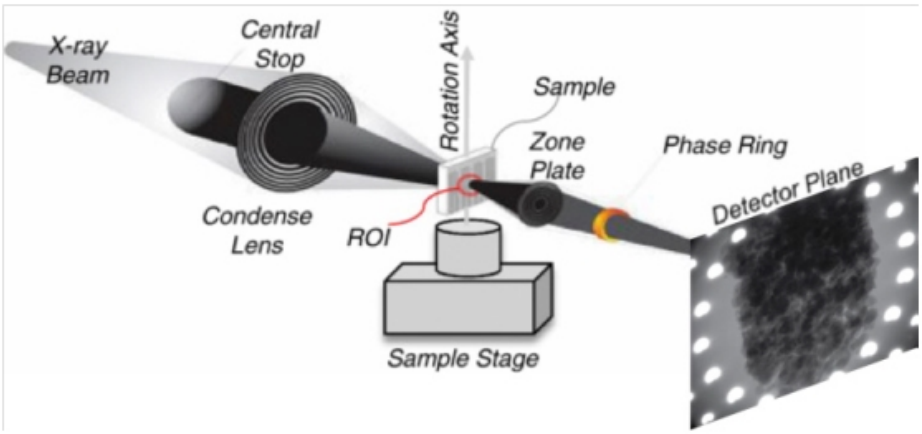

Figure 3.1. Schematic of an x-ray computed tomography

A set of x-ray projected images is generated through the following steps. First, filtered x-ray sources are compensated for the lack of flux through a high efficiency reflective capillary condenser lens, and then the x-rays penetrate an object through as much as 100 μm as the sample thickness limitation depends on the material. Second, Fresnel zone plates focus x-rays by means of diffraction to make a high resolution image. The resolution of the zone plate based x-ray microscope is independent of x-ray source spot size and is ultimately limited by the outermost zone width of the zone plate such that finer zones give higher resolution [23]. Third, the phase ring increases the contrast in transmission x-ray imaging for low Z materials. After that, the x-rays arrive on the scintillator detector and are projected on the CCD. Lastly, the sample object is rotated at 0.25 degree rotation increment over 180 degree to capture the next projected image [24].

The hard part of the experiment is how to get a perfect sample. Because the sample is weak and easy to break, and we have to break it by hand, it is pretty hard to get a top angle we want to use. The perfect angle should be 60 degree, so that the camera can take the full view of the material. Moreover, three materials were prepared for the Argonne trip, which include $LiCoO_2$, $LiMn_2O_4$, and NMC+LTAP.

It is hard to make a sample of $LiMn_2O_4$ and NMC+LTAP, because they are easy to break into powder.

Then, an image processing method, which is the responsibility of my group mate C. Lim, is going to briefly described.

An x-ray projected image from a synchrotron nano-CT is shown in Figure 3.2(a). A sinogram data is obtained by stacking all angles of the projected images together. A section of the sinogram is shown in Figure 3.2(b). To reconstruct the electrode geometry, the sinogram is transformed in Cartesian coordinate system by employing the python based framework TomoPy. Figure 3.2(c) shows the transformed image at the height of the section A-A on Figure 3.2 (a). Bright color regions with high intensity values represent the active particles of the electrode, while the rest of the image is regarded as the pore, carbon electric conductor, and binder phases of the cathode electrode. A 3D volume data can be obtained by stacking the transformed image set using the Insight Toolkit (ITK) which is an image processing library based on C++. Moreover, volumetric mesh of the porous structure can be obtained from iso2mesh Matlab codes as shown in Figure 3.2(d).

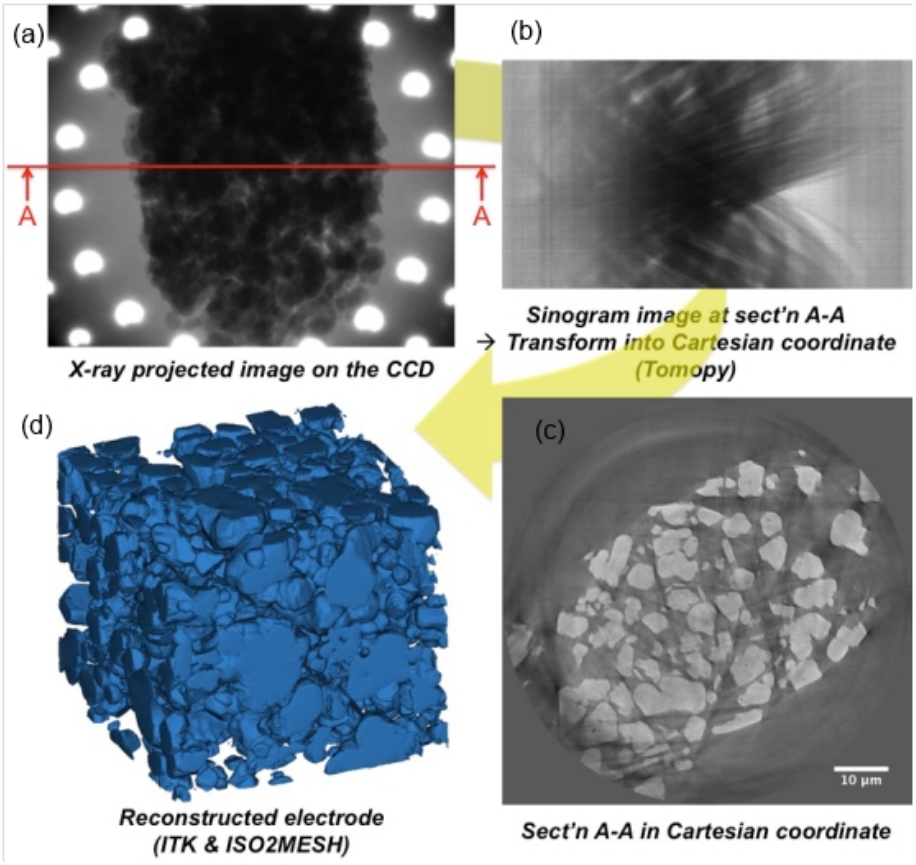

Figure 3.2. Porous structure reconstruction process by open-source toolkits

4. 3D MODEL SIMULATION

In the past several years, numerical studies have been conducted to investigate the morphological effects on the performance of LIBs. For example, Smith et al. developed a two dimensional (2D) ion transport model using scanning electron microscope (SEM) images of LIB electrodes [9,25]. These numerical studies elucidated the effects of the electrodes microstructure on battery performance. However, the 2D model and the assumed microstructure do not represent the real complex morphology of LIB electrodes.

Because of the limitation of the pseudo 2D model, we also tried to figure out the simulation of 3D model. Pseudo 2D model assumes the pores are uniform, in other words, the geometry of pores are ignored. In the pseudo 2D model, lithium ions go through the electrodes in a straight line, but that is not true. In the real structure, the channel is cragged. To make up for this fault, the 3D model based on real structure is necessary. It is also what we talked about in the last part.

The next step is using the 3D model to simulate the heat of mixing again under the same parameters. Then compare the results. The simulation of the 3D model was run in the self-built software by Bo Yan [3]. The platform for this simulation is on C++.

The main parameters are the same as the standard pseudo 2D model, whose parameters are shown in Table 1.1. The only difference is the diffusivity.

4.1 New Diffusivity Function

Compared to the 3D model results, the heat of mixing across the electrolyte in the 1D model is much higher. This is because the diffusivity of the electrolyte is different. In the 3D model, the diffusivity is a function which is relative to the concentration

and temperature change. But in the 1D model, the electrolyte diffusivity is a constant from the material reference.

After we checked through the literature, we found that the diffusivity could be very different in the different references. Therefore, we decided to redo some of the cases of 1D model to compare with the 3D model simulation results.

Function:

$$\log\left(\mathrm{D_e}\right) = 4.43 - 54\left(\mathrm{T} - 5 \times 10^3 \mathrm{c_e} - 229\right) - 0.22 \times 10^3 \mathrm{c_e} \tag{4.1}$$

where D_e is the diffusivity, c_e is the local concentration.[5]

4.2 Charging and Discharging for Different C Rates

1C discharge:

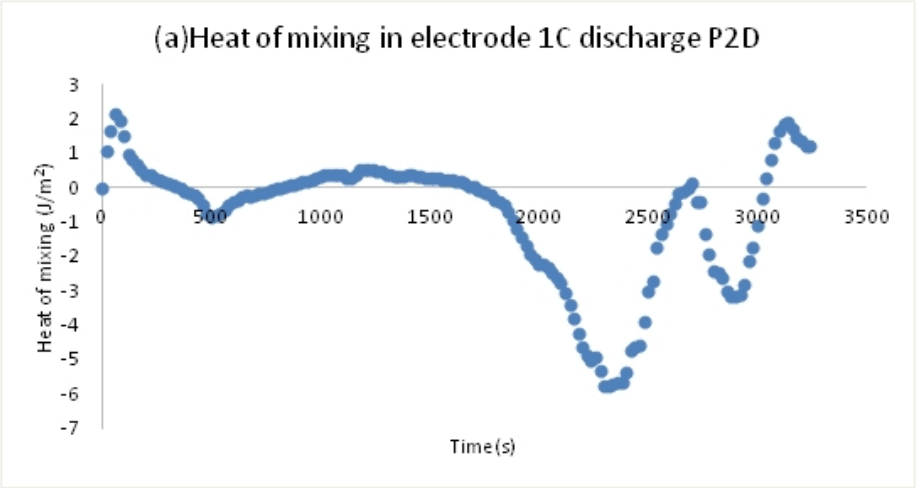

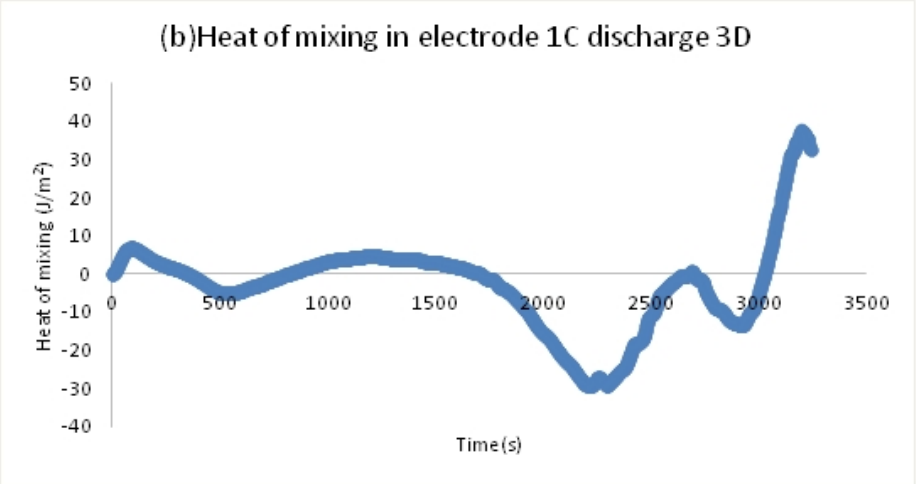

Figure 4.1. P2D and 3D model results of heat of mixing for 1C discharge

5C discharge:

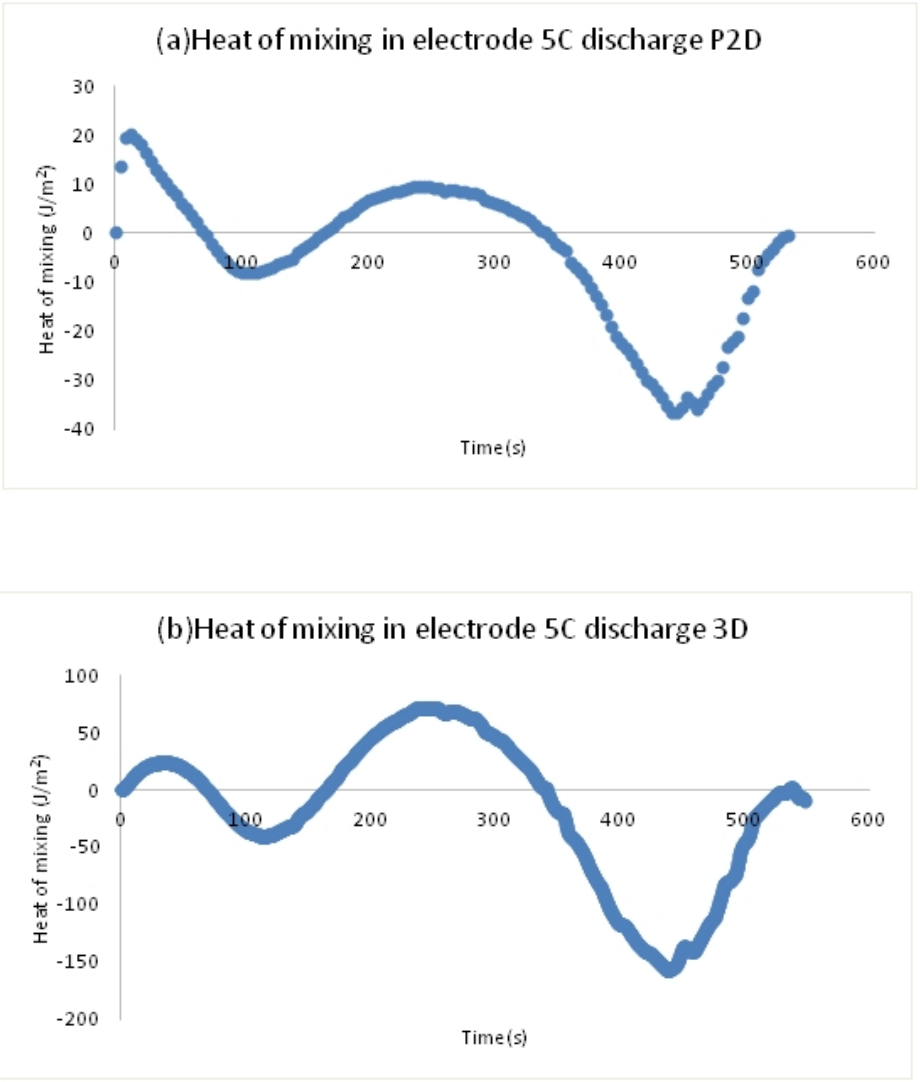

Figure 4.2. P2D and 3D model results of heat of mixing for 5C discharge

In the 3D model results, the curve trends and magnitude are the same as the results of the pseudo 2D model. This means the results are comparable. Then the Figures 4.1-4.2 show that the values of 3D model results are larger than the 2D results. Because of the irregular particle shape, particle size distribution, and packing pattern in 3D structure model, the concentration gradient in 3D model is much larger than it in P2D model. A simple structure of 3D model is shown in Figure 4.3. The irregular particle shape lead to the concentration distribution is not uniformed within particles. The different particle size lead to the larger concentration gradient in the electrode. All of these factors make the heat of mixing in 3D model larger than it in P2D model.

Figure 4.3. Simple structure of particles in 3D model

4.3 Summary

After comparing the results from the pseudo 2D model and the 3D model, the magnitudes are the same. The curves trends are also similar. Through analyze, the heat of mixing results from 3D model are 3 - 5 times larger than the results from the P2D model. The factors that made these differences are the irregular particle shape, particle size distribution, and the packing pattern, which cause the larger concentration gradient within particles and across electrode. On the other hand, the relationship between 3D and P2D results are the same in each case. It proves the results from 3D model are reliable. At last, because the heat of mixing in the 3D model is much larger than it in the P2D model, it also proves the heat of mixing is important to be considered in the real situation.

5. CONCLUSIONS AND FUTURE WORK

5.1 Conclusions

Heat of mixing was usually ignored during the simulation and design, and even in safety consideration. Through this work, we found it is meaningful to consider at some time.

From the above results, heat of mixing is influenced by C rate, particle size, porosity, and thickness. These are the parameters we can control during the manufacturing procedure and charging or discharging process. To conclude the effect, heat of mixing not only increases with C rate and thicknesss increasing, but also increase with particle size and porositys decreasing. Based on these simulations, we can know how to control the heat of mixing change when it is necessary.

In the comparison of heat of mixing and total heat, heat of mixing is quite small. It is usually lower than 10 percent of the total heat, sometimes even lower than 1 percent. Therefore, heat of mixing is not as important as resistive heat or reaction heat, but it is important to consider it when the other heat sources are also small.

Moreover, the heat of mixing is caused by concentration gradient, so it does not rely on external potential and current. It still exists after the charging or discharging process has been stopped. In that case, it has to be considered.

After comparing the results from pseudo 2D model and 3D model, it show the heat of mixing is larger than we expected in the real situation. The 3D model simulation helps to know the magnitude of heat of mixing in 3D structure. It also shows the influence of particle shape and particle size distribution to heat of mixing. It is closer to the real situation.

5.2 Future Work

There is some more work that can be done in the future to improve the current mathematical model of LIBs as shown below.

- Use the 3D model to simulate the heat generation again.
- The temperature change should be considered in the next simulation. Temperature was set as a constant that equal to 298K in this research, but some parameters will change with temperature, such as OCP, dU/dT.
- Compare the simulation results with some reliable experimental data to see whether they are the same. If not, investigate the contributing factors.

REFERENCES

REFERENCES

[1] L. Saw, K. Somasundaram, Y. Ye, and O. Tay, "Electro-thermal analysis of lithium iron phosphate battery for electric vehicles," *Journal of Power Sources*, vol. 249, no. 2, pp. 231–238, 2014.

[2] K. E. Thomas and J. Newman, "Thermal modeling of porous insertion electrodes," *Journal of the Electrochemical Society*, vol. 150, no. 6, pp. A176–A192, 2003.

[3] B. Yan, C. Lim, L. Yin, and L. Zhu, "Three dimensional simulation of galvanostatic discharge of $licoo_2$ cathode based on x-ray nano-ct images," *Journal of the Electrochemical Society*, vol. 159, no. 1, pp. A1604–A1614, 2012.

[4] K. E. Thomas, C. Bogatu, and J. Newman, "Measurement of the entropy of reaction as a function of state of charge in doped and undoped lithium manganese oxide," *Journal of the Electrochemical Society*, vol. 148, no. 6, pp. A570–A575, 2001.

[5] K. Kumaresan, G. Sikha, and W. R.E, "Thermal model for a li-ion cell," *Journal of The Electrochemical Society*, vol. 155, pp. A164–A171, 2008.

[6] J. Mao, W. Tiedemannand, and J. Newman, "Simulation of li ion cells by dualfoil model under constant-resistance load," *Journal of The Electrochemical Society*, vol. 58, pp. 71–81, 2014.

[7] L. Rao and J. Newman, "Heat generation rate and general energy balance for insertion battery systems," *Journal of The Electrochemical Society*, vol. 144, pp. 2697–2704, 1997.

[8] M. Xiao and S. Choe, "Theoretical and experimental analysis of heat generations of a pouch type $limn_2o_4$/carbon high power li-polymer battery," *Journal of Power Sources*, vol. 241, pp. 46–55, 2013.

[9] M. Xu, Z. Zhang, X. Wang, L. Jia, and L. Yang, "Two-dimensional electrochemicalthermal coupled modeling of cylindrical $lifepo_4$ batteries," *Journal of Power Sources*, vol. 256, pp. 233–243, 2014.

[10] M. Doyle and Y. Fuentes, "Computer simulations of a lithium-ion polymer battery and implications for higher capacity next-generation battery designs," *Journal of the Electrochemical Society*, vol. 150, p. A706, 2003.

[11] L. Cai and R. E. White, "Mathematical modeling of a lithium ion battery with thermal effects in comsol inc. multiphysics (mp) software," *Journal of Power Sources*, vol. 169, pp. 5985–5989, 2011.

[12] X. Zhang, "Multiscale modeling of li - ion cells: Mechanics, heat generation and electrochemical kinetics." Ph.D dissertation, The University of Michigan, 2009.

[13] U. Kim, J. Yi, C. B. Shin, T. Han, and S. Park, "Modelling the thermal behaviour of a lithium-ion battery during charge," *Journal of Power Sources*, vol. 196, pp. 5115–5121, 2011.

[14] N. Baba, H. Yoshida, M. Nagaoka, C. Okuda, and S. Kawauchi, "Numerical simulation of thermal behavior of lithium-ion secondary batteries using the enhanced single particle model," *Journal of Power Sources*, vol. 252, pp. 214–228, 2014.

[15] F. Jiang, P. Peng, and Y. Sun, "Thermal analyses of $lifepo_4$/graphite battery discharge processes," *Journal of Power Sources*, vol. 243, pp. 181–194, 2013.

[16] Y. Saito, M. Shikano, and H. Kobayashi, "Heat generation behavior during charging and discharging of lithium-ion batteries after long-time storage," *Journal of Power Sources*, vol. 244, pp. 294–299, 2013.

[17] Q. Zhang and R. White, "Moving boundary model for the discharge of a $licoo_2$ electrode," *Journal of the Electrochemical Society*, vol. 154, p. A587, 2007.

[18] J. Christensen and J. Newman, "A mathematical model of stress generation and fracture in lithium manganese oxide." *Journal of the Electrochemical Society*, vol. 153, pp. A1019–A1030, 2006.

[19] J. Reimers and J. Dahn, "Nato reference mobility model, edition 1 user's guide," *Journal of Solid State Electrochemistry*, vol. 10, p. 293, 2006.

[20] X. Zhang, W. Shyy, and A. Sastry, "Numerical simulation of intercalation-induced stress in li-ion battery electrode particles." *Journal of the Electrochemical Society*, vol. 154, pp. A910–A916, 2007.

[21] C. K. Chan, H. Peng, G. Liu, K. McIlwrath, X. F. Zhang, R. A. Huggins, and Y. Cui, "High-performance lithium battery anodes using silicon nanowires," *Nature nanotechnology*, vol. 3.1, pp. 31–35, 2008.

[22] S. J. Harris, A. Timmons, D. Baker, and C. Monroe, "Direct in situ measurements of li transport in li-ion battery negative electrodes," *Chemical Physics Letters*, vol. 485, no. 4, pp. 265–274.

[23] W. Chen, K. Yu-chen, J. Cronin, Q. Yuan, K. Yakal-Kremski, S. A. Barnett, and J. Wang, "3d non-destructive morphological analysis of a solid oxide fuel cell anode using full-field x-ray nano-tomography," *Journal of Power Sources*, vol. 115, pp. 131–139, 2012.

[24] C. Lim, "Three dimensional geomatric effects on the electrochemical performance of lithium ion batteries." Ph.D dissertation, Purdue University, Indianapolis, 2015.

[25] T. Hutzenlaub, S. Thiele, N. Paust, R. Spotnitz, R. Zengerle, and C. Walchshofer, "Three-dimensional electrochemical li-ion battery modelling featuring a focused ion-beam/scanning electron microscopy based three-phase reconstruction of a $licoo_2$ cathode," *Electrochimica Acta*, vol. 115, pp. 131–139, 2014.